HHS Public Access

Author manuscript

Nat Neurosci. Author manuscript; available in PMC 2021 July 25.

Published in final edited form as:

Nat Neurosci. 2021 March ; 24(3): 379–390. doi:10.1038/s41593-020-00772-7.

Ventral arkypallidal neurons inhibit accumbal firing to promote reward consumption.

Yvan M. Vachez[1,*], **Jessica R. Tooley**[1,*], **Kavitha Abiraman**[1], **Bridget Matikainen-Ankney**[2], **Eric Casey**[2], **Tom Earnest**[1,2], **Leana M. Ramos**[5], **Hanna Silberberg**[5], **Elizabeth Godynyuk**[1,2], **Olivia Uddin**[3], **Lauren Marconi**[4], **Claire E. Le Pichon**[5], **Meaghan C. Creed**[†,1,2,6]

[1.]Department of Anesthesiology, Washington University Pain Center, Washington University School of Medicine, St. Louis, Missouri [2.]Department of Psychiatry, Washington University School of Medicine, St. Louis Missouri [3.]University of Maryland, Department of Anatomy and Neurobiology, Baltimore Maryland [4.]University of Pennsylvania, Perelman School of Medicine, Philadelphia Pennsylvania [5.]Eunice Kennedy Shriver National Institute of Child Health and Human Development, National Institutes of Health, Bethesda Maryland [6.]Departments of Neuroscience and Biomedical Engineering, Washington University School of Medicine, St. Louis, Missouri

Abstract

The shell of the nucleus accumbens (NAcSh) and ventral pallidum (VP) are critical for reward processing, although how coordinated activity within these nuclei orchestrates reward valuation and consumption remains unclear. Inhibition of NAcSh firing is necessary for reward consumption, but the source of this inhibition remains unknown. Here, we report that a subpopulation of VP neurons, the ventral arkypallidal (vArky) neurons, project back to the NAcSh, where they inhibit NAcSh neurons in vivo in mice. Consistent with this pathway driving reward consumption via inhibition of the NAcSh, calcium activity of vArky neurons scaled with reward palatability and predicted the subsequent drinking behavior during a free-access paradigm, which was dissociable from reward seeking. Activation of the VP to NAchSh pathway increased on-going reward consumption while amplifying hedonic reactions to reward. Our results establish a pivotal role of vArky neurons in promoting reward consumption, through modulating NAcSh firing in a value-dependent manner.

[†]Correspondence: Meaghan C. Creed, meaghan.creed@wustl.edu.
[*]Equal contribution

Author contributions: YMV, KA and MCC wrote the paper with input from all authors. YMV, JRT, LM, LMR, HS and TE performed anatomical experiments; YMV, KA and MCC performed patch clamp physiology, MCC, JRT and OU performed in vivo electrophysiology, YMV, JRT and EG performed fiber photometry, YMV, JRT, EC and KA performed behavioral experiments. BMA engineered custom hardware for behavioral experiments, BMA and TE developed analyses methods. Data was analyzed by YMV, JRT, KA and MCC. Work was supervised by BMA, CEL and MCC.

Competing interests statement: Authors report no financial interests or conflicts of interest.

Data availability statement: The data that support the findings of this study are available from the corresponding author upon request. Analysis code will be provided from authors upon request.

Introduction

The ventral basal ganglia is a collection of interconnected subcortical nuclei critical for reward processing and generating goal-directed behaviors[1]. The nucleus accumbens (NAc) and ventral pallidum (VP) are two key nuclei within this network, and are crucial for reward valuation and consumption[2]. The NAc shell (NAcSh) is composed of medium spiny neurons expressing the D1- or D2-dopamine receptor (D1-MSNs, D2-MSNs, respectively), which both densely innervate the VP[3,4]. The VP is therefore considered the primary output nucleus of the NAcSh[3,5]. A large fraction of neurons in the medial subdivision of NAcSh specifically neurons are inhibited during reward consumption, and this inhibition is both necessary and permissive for reward consumption[6,7]. The magnitude of this inhibition scales with reward value[6,8,9] and is hypothesized to produce motivational drive by disinhibition of downstream targets, including the VP[1,10]. Despite its critical role in reward consumption, the neural substrate driving this inhibition of NAcSh firing is still poorly understood.

While the VP is classically considered an output structure of the NAc, this has been challenged by neuroanatomical studies and recent functional evidence. Specifically, tract-tracing has demonstrated the existence of projections from the VP to the NAc in rodents[11,12] and primates[13]. Similar anatomy has been described in the dorsal basal ganglia, where projections from the external globus pallidus to dorsal striatum have been coined “arkypallidal” due to their dense net-like projections impinging broadly through the dorsal striatum[14,15,16]. Functionally, neural responses to reward-consumption and to cues that predict reward also emerge with shorter latency in the VP neurons to NAc neurons[17,18,19,20,21]. Based on this work, we hypothesized that back projections from the VP may be the source of inhibition to the NAcSh that promotes reward consumption. This ventral arkypallidal pathway (vArky; from VP to NAcSh) may drive reward-related inhibition in NAcSh firing, and could reconcile the different latencies with which reward-related signals arise in these two nuclei.

Here, we demonstrate that vArky neurons send dense inhibitory projections to NAcSh MSNs and interneurons (INs), and this inhibitory drive contributes to reward-consumption-related neuronal responses in the NAcSh. The endogenous activity of vArky neurons predicts the volume of subsequent reward consumption and promotes reward consumption by increasing hedonic value of reward. We thus describe a distinct behavioral function of ventral arkypallidal neurons, while providing new insights into information flow in the ventral basal ganglia necessary for understanding reward processing.

Results

NAcSh inhibition promotes reward consumption

Inhibition of the NAcSh during reward consumption has been consistently documented, despite heterogeneity across paradigms regarding operant contingencies, method of responding, and metabolic state[6,22,23,24,25]. Here, in a free-access paradigm, when sated mice drink from a lickometer, 36% of recorded NAcSh neurons were inhibited during reward consumption (Fig1a–d). Also consistent with prior work, the responses during reward approach were heterogeneous, with 7% of neurons showing a decrease and 25.0% an

increase (Extended data 1a–d). Further, NAcSh inhibition was sufficient to drive reward consumption, as closed-loop optogenetic inhibition with Arch3.0 triggered by reward consumption increased the total reward consumption time, number of bouts, and average bout length (Fig 1e–h, Extended data 2a–d). NAcSh inhibition did not induce a place preference or induce locomotor effects (Extended data 2e,f), demonstrating that this inhibition has selective effects on reward consumption. However, the source of this inhibition is not known. We hypothesized that the VP is the dominant source of inhibition to the NAcSh, given its established role in encoding motivation and reward value[19,26,27], and the earlier onset of value signals in the VP relative to the NAc[17,18,19,21].

vArky neurons inhibit the NAcSh

To characterize the anatomy of projections from the VP to NAcSh, we injected retrograde-AAV expressing Cre into the NAcSh, and cre-dependent ChR2-tagged to eYFP into the VP (Extended data 3a). We confirmed that cell bodies in the subcommisural VP were labelled, and that eYFP+ terminals were abundant in the NAcSh (Extended data 3b,c); fluorescence signal and length of labeled axons in the NAcSh was significantly greater than all other brain regions examined (Extended data 3d,e, Vid1). We refer to these NAcSh-projecting VP neurons as ventral arkypallidal (vArky) neurons, given their dense, net-like morphology (Vid1), reminiscent of the arkypallidal projection from globus pallidus to striatum in the dorsal basal ganglia[14,15].

While the VP is predominantly GABAergic, we and others have recently shown that glutamatergic VP neurons constitute a distinct population of projection neurons[28,29]. To determine whether the vArky pathway is comprised of GABAergic or glutamatergic neurons, we injected retrobeads in the NAcSh and measured co-expression of VP retrobeads with SLC32A1 (encoding vesicular inhibitory amino acid transporter, VIAAT) and SLC17A6 (encoding vesicular glutamate transporter 2, VGluT2) mRNA using fluorescent in situ hybridization (fISH, Fig 2a,b). We found 86.6% of retrobead-positive neurons co-localized with VIAAT, consistent with early anatomical studies[12]; there was no co-localization between retrobeads and VGluT2 (Fig 2a–c).

The NAc is composed of D1- and D2-MSNs, as well as interneurons. To determine the post-synaptic targets of vArky neurons within the NAcSh, we used complementary approaches of retrograde genetic tracing and anterograde circuit mapping. Retrograde tracing using G-deleted rabies virus seeding in the NAcSh (Fig 2d) revealed that normalized counts of EGFP-labelled cells in VP were significantly denser in D1-Cre and A2a-Cre mice relative to PV-Cre and ChAT-Cre mice (Fig 2e–g), reflecting greater monosynaptic inputs from VP onto MSNs relative to interneurons. Consistent with prior anatomical tracing, our data reveal that these neurons were concentrated around the anterior-medial, subcomissural VP, with only sparse labeling in caudal VP (Churchill and Kalivas, 1994); Fig 2g). We corroborated these results using functional circuit mapping, by injecting ChR2 into the VP, and recording light-evoked responses in NAcSh D1-MSNs, D2-MSNs, parvalbumin- (PV) or cholinergic interneurons (CINs) using patch-clamp electrophysiology (Fig 3a,b and Extended data 4a,b). Most MSNs (84% of D1- and 79% of D2-MSNs) but only a minority of interneurons (30% of CINs and 28% of PVs) received VP input (Fig 3c,d). There was no difference in

connectivity rate (Fig 3d), amplitude or release probability (Fig 3e, Extended data 4c,d) as a function of location within the NAcSh. The latency to current peak and the insensitivity of this latency to tetrodotoxin confirm that these currents are monosynaptic (Fig 3f,g). Consistent with our fISH results, light-evoked currents were blocked by picrotoxin, but not by APV/NBQX, confirming their exclusively GABAergic nature (Fig 3h,i).

While these experiments establish that the VP makes dense, inhibitory, mono-synaptic connections onto NAcSh neurons, these post-synaptic neurons make extensive local connections. Therefore, poly-synaptic network effects of stimulation of vArky neurons on NAcSh activity *in vivo* would not be evident in the slice preparation. To address this limitation, we transfected the VP with ChR2 as in our slice experiments, and implanted an optic fiber coupled to a recording array in the NAcSh (Fig 4a,b, Extended data 5a). We recorded 32 multi units and 23 single units from 6 freely moving mice. Single units were classified as putative MSNs (pMSNs) or interneurons (pINs) according to firing rate (FR), waveform peak-valley duration (P-V) and coefficient of variation (CV) in firing rate. Among the recorded single units, 9 putative MSNs and 14 putative interneurons were identified (Fig 4c, Extended Data 5b–d, MSN FR = 0.40 ± 0.11 Hz, P-V = 462.8 ± 27.96 μs, CV = 1.77 ± 0.254, IN FR = 3.53 ± 1.20 Hz, P-V = 242.01 ± 26.27 μs, CV = 1.23 ± 0.17). Overall, 53.62% of units were light-modulated, with the vast majority of these units (91.89%) exhibiting a significant *decrease* in firing rate in response to VP terminal activation, consistent with the GABAergic nature of this projection; a modest increase in firing rate was observed in 3 multi-units in response to a 1 sec or 15 msec light pulse (Fig 4d–h, Extended data 5e–h). There was no difference in the proportion of light-modulated units between multi-units, pMSNs or pINs, nor was there a significant difference in the magnitude of inhibition between these unit classes (Fig 4f–h). These results demonstrate that activation of VP terminals in the NAcSh is sufficient to robustly inhibit NAcSh firing in vivo.

Endogenous vArky calcium is associated with duration of reward consumption

Given that vArky neurons inhibit NAcSh neurons in vivo, and that NAcSh inhibition drives reward consumption[7,25] (Fig 1), we hypothesized that vArky neurons are a source of NAcSh inhibition during natural reward consumption. We therefore predicted that their activity would increase during reward consumption and the strength of this activity at the onset of consumption would corelate with length of ensuing lick bouts. To test this, we expressed GCaMP6s exclusively in vArky neurons using a retrograde viral strategy, and recorded bulk calcium activity using fiber photometry (Fig 5a). We aligned calcium activity to the onset of lick bouts during a free-access task, and determined that, as predicted, fluorescence peaked following the onset of reward consumption; there was no lick-related fluorescence change in GFP-controls (Fig 5b). To determine whether the vArky calcium activity predicts the duration of subsequent reward consumption, we calculated the area under the curve (AUC) of the first second following the onset of reward consumption, and for each subject, split the trials into upper (GCaMP high trials) and lower quartiles (GCaMP low trials; Fig 5c, Extended data 6a–e). Consistent with our hypothesis, GCaMP high trials were associated with significantly *longer* durations of licking than GCaMP low trials (Fig 5c,d). This relationship was observed across every subject, but not in GFP controls (Extended data 6c–e). To confirm the significance of this behavioral difference, we performed a permutation

analysis in which we shuffled the assignment of high- and low-GCaMP trials 2000 times, and detected an average difference of 0.6% in lick duration vs. 42.6% in the unshuffled data (Fig 5e). Importantly, the vArky calcium signal began to ramp during reward approach, peaking after reward consumption. Conversely, and consistent with our in vivo recordings, calcium signal in the NAcSh decreased during reward consumption, which began only after reward consumption onset (Extended data 7a–d). While a direct comparative analysis is not possible as these recordings were performed in separate animals, the increase in vArky calcium activity before consumption onset is consistent with the role of the vArky pathway providing inhibitory drive to the NAcSh.

In addition, we determined that vArky activity was not related to reward seeking per se by introducing a requirement for a nose poke before reward availability on a fixed-ratio 1 schedule (Extended data 8a). We recorded vArky calcium signal after 3 sessions of overnight training, and found no significant change in GCaMP signal preceding or immediately following the seeking nose-poke, prior to reward consumption, or around inactive nose pokes (Fig 5f,g). Fluorescence signal peaked upon pellet retrieval, confirming that vArky neuronal activity is not associated with the motor act of licking, but is consistent with a reward consumption signal (Extended data 8a–c). We performed three additional analyses to rule out the possibility that the reward consumption responses were driven by motor-related activity in vArky neurons that may occur during reward approach. We first aligned the photometry signal to locomotor arrests. In contrast to the *increase* in signal around reward consumption, there was no significant change in the fluorescence signal with locomotor arrests not associated with reward consumption (Extended data 8d). There was also no significant change in GCaMP signal related to locomotor initiations or to peaks in velocity (Extended data 8e,f). These results confirm that the calcium response in vArky neurons is specific to the onset of reward consumption, and the magnitude of this response predicts the duration of ensuing lick bout.

Activation of vArky neurons promotes reward consumption

To test our conclusion that activation of vArky neurons determines the duration of lick bouts, we applied closed-loop optogenetic stimulation to drive vArky activity at 20 Hz during reward consumption in a free-access paradigm (Fig 6a, Extended data 9a,b). This frequency was chosen after recording vArky neurons ex vivo, where we determined that all vArky neurons were consistently able to fire at frequencies above 20 Hz (maximum firing frequency: 55.1 ± 6.7 Hz, range: 22-91 Hz, Extended data 10a–d).

Closed-loop stimulation of vArky terminals significantly increased the total drinking time (214%, Fig 6b). Consistent with our prediction, this effect was not due to changes in the number of bouts (Fig 6c), but was driven by an increase in mean bout length (Fig 6d,e). Importantly, open-loop optogenetic vArky stimulation applied randomly throughout the session did not increase drinking time or number of lick bouts (Fig 6b–d), confirming that vArky stim does not drive approach behavior, but rather promotes on-going reward consumption. Moreover, when a spout without liquid was presented, closed-loop vArky stimulation did not alter the total time interacting with this spout, the number of interactions or mean interaction length (Fig 6f–h). vArky stimulation also did not affect locomotor

activity in either eYFP- or ChR2-injected mice, nor induce a place preference in real-time-place-preference task (Extended data 10c–d). Together, these results argue that the increase in reward consumption with vArky stimulation is not due to reinforcing the action of licking, to inhibition of locomotor activity or to a rewarding effect of the stimulation itself (Extended data 9d).

Selective inhibition of vArky neurons attenuates reward-related inhibition of NAcSh neurons and reward consumption.

To determine whether activity of vArky neurons is required for consumption-related NAcSh inhibition we used a retrograde viral strategy to express the inhibitory opsin, archaerhodopsin (Arch3.0), selectively in NAcSh-projecting VP neurons, and inhibited their activity in a closed-loop paradigm while recording NAcSh units (Fig 7a, Supplemental Fig 1a–c). These were recorded in a single session during which epochs of Arch3.0 stimulation were interleaved with non-stimulated trials (Fig 7b). As predicted, vArky inhibition attenuated the consumption-related inhibition in NAcSh firing (Fig 7c). We examined reward-consumption behavior using this same Arch3.0-mediated inhibition approach and found that closed-loop vArky inhibition significantly decreased total drinking time (Fig 7d), without affecting the number of reward approaches (Fig 7e). Consistent with our optogenetic activation results, vArky inhibition significantly decreased the mean bout length of drinking behavior (Fig 7f) and shifted the distribution towards shorter drinking bouts (Fig 7g). Together, these results support the importance of vArky neurons for maintaining reward-related NAcSh inhibition and for sustaining on-going reward consumption.

vArky activity reflects and promotes reward palatability

Reward consumption is driven by dissociable processing of “wanting” (motivation for reward) and “liking” (hedonic value of reward[30]). The selective increase in bout length without a change in the approach behavior indicates stimulation of vArky terminals in the NAcSh increased the palatability of reward, rather than changed motivation for reward per se[31]. We tested this explicitly in two additional tasks. We first measured orofacial reactivity in response to a 10% sucrose solution (Vid2). vArky stimulation increased post-ingestive hedonic tongue protrusions during stimulation relative to un-stimulated trials (Fig 8a), suggesting increased hedonic value of reward. Further, when two identical liquid rewards were presented in a two-bottle choice paradigm (Fig 8b), significantly more mice exhibited a preference for the bottle paired with optogenetic vArky stimulation relative to EYFP controls (Fig 8c). We also determined that while mice exhibited longer drinking times on the stimulation-paired bottle throughout the session (Fig 8d), the proportion of approaches to the stimulation-paired bottle also increased over the course of the session (Fig 8e). This gradual emergence of an approach bias over the course of the session suggests the vArky stimulation modulates the value of the contents of the stimulation-paired bottle, rather than driving reward approach.

While vArky stimulation does not induce a place preference (Extended Data 10d) or support self-stimulation on its own (Fig 8f), it is possible that when paired with exogenous reward, vArky stimulation becomes sufficient to reinforce the specific action of responding on the stimulation-paired bottle, as has been reported for stimulation of dopamine neurons[32,33].

This is an important caveat to the two-bottle choice task above, and so we further investigated whether vArky activity is related to hedonic value of reward, by manipulating reward value and measuring vArky calcium signal in head-fixed mice (Fig 8g–I). In this paradigm, 20 μL of 5% sucrose, water or low concentration of quinine solution (0.05%) was intraorally infused, and the number of infusions was balanced for each solution (Fig 8g). The low quinine concentration was chosen to ensure participation in the task, however in a subset of trials, mice rejected the quinine, and it was not consumed. Under these conditions, vArky calcium activity scaled with reward value, with AUC, peak height and half-life of decay ($t_{1/2}$) all being highest in sucrose, followed by water then quinine. Critically, on trials where quinine was rejected, GCaMP signal decreased relative to baseline, bolstering the interpretation that vArky calcium activity reflects value of the solution (Fig 8h–l). GFP signal showed no changes around lick bouts or liquid infusions (Fig 8i). Together, these results support a model by which the vArky pathway promotes reward consumption by amplifying the hedonic value of reward.

Discussion

The NAc and VP have been extensively implicated in reward seeking and processing, while prior chemogenetic functional disconnection studies of the NAcSh and VP has suggested that coordinated activity between these structures is involved in cue-triggered reward seeking, but does not alter reward consumption[34,35]. It is important to note that we focused our manipulations on the medial NAcSh specifically, which is known to play a robust role in coding hedonic value[2,36]. Moreover, interpretation of disconnection studies has been complicated by the lack of directionality of the manipulation, and to date, no published studies have selectively activated the vArky pathway to determine its effect on reward-related behavior. A lack of prior anatomical knowledge of this pathway has further limited our understanding of the reciprocal interactions between the NAc and VP. Analogous to the organization that has been described in the dorsal basal ganglia[16], vArky neurons send dense, web-like processes throughout the NAcSh, forming inhibitory synapses onto the majority of NAcSh MSNs and more sparsely onto interneurons. vArky activation is sufficient to inhibit putative NAcSh MSNs and interneurons in vivo (Fig 4, Extended data 5), which is critical, since inhibition of NAcSh MSNs is both necessary and permissive for reward consumption[6,7]. While we did not examine the effect of vArky neurons on cue-triggered reward seeking, the inhibition of CINS by vArky neurons could invigorate salience of reward-predictive cues by modulating local cholinergic and dopamine tone[37,38]. Conversely, vArky modulation of PVs may sculpt reward-related activity in functional neuronal ensembles in the NAcSh. This possibility is interesting in light of our in vivo electrophysiology results; a minority of NAcSh neurons increased firing in response to vArky terminal activation. This is likely due to release of lateral inhibition from inhibited PVs or MSNs. Future work will establish whether these activated units represent a functional ensemble or play a unique role in reward processing, consistent with observed subsets of NAcSh units that increase firing in response to reward[17].

Decreased excitatory drive is another potential substrate of reward-related NAcSh inhibition. Activity of excitatory projections from thalamus, hippocampus and amygdala to NAcSh is reduced during reward consumption, while inhibition of these excitatory inputs produces

appetitive motivation[9,39,40]. In contrast, we found no evidence for vArky neurons modulating reward approach or appetitive motivation. vArky stimulation does not promote reward approach, nor does it support self-administration or place preference in the absence of reward. Moreover, activation of GABA receptors in the NAcSh enhances hedonic value of reward, while modulation of accumbal excitatory tone does not have this effect [9,41]. We demonstrate that the VP is an important source of exogenous GABA to the NAcSh that amplifies reward palatability. In addition to the VP, the VTA and LH are also potential sources of GABAergic input to the NAcSh[42,43] (Supplemental figure 2). However, while stimulation of vArky terminals in the NAc promote reward consumption, chemogenetic inhibition of NAc-projecting VTA GABA neurons does not affect reward responding[44], and optogenetic stimulation of these neurons does not affect free consumption when applied in a closed-loop manner as we have done here[45]. The reason for these different behavioral effects likely arises because GABAergic afferents from VTA to the NAc target CINs nearly exclusively, with very sparse innervation of MSNs[37]. It is unclear whether LH terminals to the NAc mediate reward consumption, and the post-synaptic targets in the NAc are not known. While optogenetic stimulation of LH GABA neurons can rapidly induce eating and reward intake, these actions have been linked to actions of LH projections in the midbrain[46,47]. This highlights the unique role of GABAergic input from vArky neurons for conveying consumption-related signals to the NAcSh.

Our fiber photometry studies further support our interpretation that vArky neurons convey value-related signals to the NAc. vArky calcium activity begins to ramp during reward approach, but the magnitude of peak responses scale with reward value during free-access consumption and during head-fixed intraoral infusion, where there is no reward approach or cue. Moreover, vArky calcium activity at reward onset predicted subsequent reward consumption, further establishing activity of this pathway as a mediator of reward consumption. On trials where quinine was sufficiently aversive that mice rejected it, vArky calcium signal was significantly decreased (Fig 8 g–l), and signal is greater following sucrose infusion and water, despite controlling for the number and amount of reward. These observations strengthen the interpretation that vArky calcium activity reflects reward palatability rather than salience or a consumption signal. An important consideration is that photometry recordings only reveal bulk calcium signaling, have limited temporal resolution and do not give information about the activity of individual neurons or subpopulations. VP neurons show heterogeneous firing patterns around reward seeking and consumption, including ramping during reward approach, bursting with salient stimuli[21,48], and increased firing rates that encode reward preference, value and satiety [19,49]. Future studies will reveal whether vArky are typically active in concert or whether discrete populations convey value information and signals related to reward expectation and the sensory act consumption.

An additional future direction will be determining which brain regions innervate vArky neurons; vArky neurons are not spontaneously active in the slice preparation (Extended data 9c,d), raising the possibility that excitatory drive to these neurons may be necessary for initiating their activity. Also, while the NAc is the primary inhibitory input into the VP[3,4], we do not know whether vArky neurons specifically are innervated by MSNs from the NAcSh. If so, it is possible that once active, vArky neurons initiate a feedforward loop by decreasing inhibitory drive from upstream NAcSh MSNs onto themselves, while also

releasing downstream brain areas such as the lateral hypothalamus (LH) and the ventral tegmental area (VTA) from tonic inhibition from NAcSh MSNs[4,7,10,50]. Uncovering the source of inputs to vArky neurons and under what conditions they are active will further enhance our understanding of how the NAcSh and VP encode hedonic value and orchestrate its behavioural expression.

Together, our results establish that vArky neurons project to and inhibit the NAcSh, and that activity in this pathway sustains reward consumption by amplifying hedonic value of reward, without affecting reward approach or reinforcement per se. This supports a model by which decreased excitatory drive to the NAcSh initiates reward approach and concomitant pause in NAcSh firing, while activity of vArky neurons is important for the maintenance of this pause which is necessary for sustained reward consumption in a value-dependent manner. Integration of this pathway into models of the basal ganglia is necessary to understand how value and motivation for reward is encoded within these nuclei, and how activity across this network coordinates reward-seeking behavior.

Methods

Subjects.

Adult male and female mice (6 – 20 weeks) on a C57BL/6J background were bred in-house from stock lines obtained from Jackson Labs (D1-Cre, 129-Tg(Drd1-cre)120Mxu/Mmjax; PV-Cre, 129P2-Pvalb<tm1(cre)Arbr>/J; ChAT-Cre, 129S6-Chattm2(cre)Lowl/J; D1-To, B6.Cg-Tg(Drd1a-tdTomato)6Calak/J; PV-To, 6-Tg(Pvalb-tdTomato)15Gfng/J JAX# 027395, or wildtype C57Bl6/J) or MMRC repository (A2a-Cre; Tg(Adora2a-cre)KG139Gsat). Mice were group housed (2 – 5/cage, single sex) in a vivarium that was controlled for humidity, temperature, and photoperiod (12 : 12; lights on at 7 am and off at 7 pm). Mice had ad libitum access to food and water throughout the experiment. All procedures were approved by the Institutional Animal Care and Use Committee at Washington University in St. Louis and the University of Maryland and were conducted in accordance with the *Guide for the Care and Use of Laboratory Animals*, as adopted by the NIH.

Stereotaxic Surgery.

Anesthesia was induced and maintained with isoflurane at 5% and 1.5%, respectively. Mice were placed in a stereotaxic frame and craniotomies were performed. For optogenetic, electrophysiology, photometry and behavioral experiments, purified and concentrated adeno-associated viruses were injected into the NAc (coordinates relative to Bregma : AP: +1.7mm, ML: −0.6mm, DV: −4.5mm), the VP (coordinates relative to Bregma, AP: +0.2 mm, ML: ±1.5 mm, DV: 4.6 mm). GCaMP6s virus (pAAV.Syn.DIO.GCaMP6s.WPRE.SV40) was obtained from Addgene, Rabies-EGFP virus (EnvA G-deleted Rabies-EGFP) was obtained from the Salk Vector Core, all other viruses (rAAV2Retro-Cre, AAV5-EF1a-DIO-hChR2(H134R)-EYFP, AAV-hSynhChR2(H134R)-EYFP, AAV-CAG-FLEX-GFP, AAV-CA-FLEX-RG, AAV-EF1a-FLEX-TVAmCherry, AAVhSyn-eArch3.0-EYFP, AAV-EF1a-DIOmCherry) were obtained from the University of North Carolina Vector Core Facility. Injections were carried out using graduated pipettes broken back to a tip diameter of 10-15 μm, at a rate of 0.05 μl / min for a total volume of

0.25-0.5 μl; pipettes were left in situ for an additional 8 minutes to allow for the diffusion of virus; 28 days was the minimum viral expression time. For behavioral experiments, optic fibers were implanted bilaterally over the NAcSh or VP and secured with 3 skull screws and dental cement. Animals recovered for at least 1 week before behavioral training, and only mice with verified infection sites and fiber placements were included in the analyses.

Neuroanatomical Tracing and Histology.

Retrograde ChR2 tracing.—250 nL of retroAAV-Cre was injected to the NAcSh, and 300 nL AAV2-DIO-hSyn-ChR2-eYFP was injected in the VP. Following 28 days expression, tissue was harvested, and ChR2 signal was amplified by immunostaining. Briefly, free floating brain sections were permeabilized in 3 washes of PBST (PBS with 3% TritonX) for 10 min each at room temperature, blocked for 1 hour in 5 % normal donkey serum in 3% PBST and then incubated in chicken anti-GFP (ThermoFisher, Cat# A10262, 1:1000)[51] overnight at 4°C. Brains were washed in 3 times in 3% PBST (10 min) and incubated in goat anti-chicken Alexa Fluor 488 (ThermoFisher, Cat# A11039, 1:1000)[51] in blocking buffer at room temperature for 2hrs. After 3 additional 10 min PBST washes and 3 washes in PBS, sections were treated with SudanBlack fluorescence quencher (Sigma) and were coverslipped and mounted using VectaShield mounting solution containing DAPI (Vector Laboratories). Intensity of fluorescence signal was quantified across 3 z-stacks from separate serial sections (20x, 500μM^2) in each of the following structures in 6 mice (2M, 4F): nucleus accumbens shell (NAcSh), ventral pallidum (VP), medial prefrontal cortex (mPFC), orbitofrontal cortex (OFC), basolateral amygdala (BLA) lateral habenula (LHb), mediodorsal thalamus (MDThal), subthalamic nucleus (STN), ventral tegmental area (VTA). To calculate axonal length, we applied a threshold to signal in the green channel reflecting ChR2 staining, axonal processes were skeletonized and traced manually by 3 independent observers, total length of all traced segments were collected in pixels and calibrated immediately to scale bars corresponding to each individual z-stack.

Immunolabeling and clearing of hemibrains by iDisco and light sheet imaging.—The iDISCO+ protocol was followed as described in previous studies[52,53] . Hemibrains were immunolabeled with Chicken anti-GFP (ThermoFisher, Cat# A10262) at 1:200 during a 5 day incubation at 37°C. Secondary antibody AlexaFluor 647-conjugated goat anti-chicken (ThermoFisher #A21449) was used at 1:200[52,53]. iDisco-processed hemibrains were imaged by light sheet microscopy (Miltenyi Biotec Ultramicroscope II) using their 4x objective. All images were acquired using the Right or Left light sheets (3 sheets per side) with dynamic focusing (10 positions) enabled. For the Dynamic Focus processing the Blend algorithm was used (Imspector software).

Retrobeads.—300 nL of Red Retrobeads and Green Retrobeads (both Lumafluor) were injected into the NAcSh (coordinates from bregma: 1.7AP, 0.6ML, −4.5DVmm) and VTA (coordinates from bregma: −3.2AP, 0.8ML, −4.3DVmm), respectively. Tissue was harvested 10 days following injection, and retrobead-expressing cells were quantified through 8 serial sections through the VP from 8 mice (5F, 3M).

Fluorescent In Situ Hybridization.—Mice were injected with green retrobeads in the NAcSh (see above) 10 days after injection, mice were euthanized and fresh tissue was frozen on dry ice, stored at −80°C and sectioned with a cryostat (Leica, CM3050) at 20 μM. Tissue was processed using RNAscope® Technology in situ hybridization assay according to provided protocols (ACDBio). Briefly, slides were transferred from −80°C and fixed with formalin, dehydrated with increasing concentrations of ethanol and pretreated with provided protease solution before hybridization with probes targeted against Slc32A1 and Slc17A6 mRNA. Following 2 h of hybridization at 40°C, sections were washed and fluorescence was amplified with provided buffer solutions. Sections were incubated with DAPI before cover-slipping for visualization.

Pseudotyped rabies tracing.—Rabies "helper virus" (AAV5-CAG-DIO-RG, AAV5-EF1a-DIO-TVA-mCherry, 250 nL in a 1:1 mixture, University of North Carolina) was injected to the NAcSh in the following Cre-driver mouse lines: ChAT-Cre, PV-Cre, D1-Cre, A2a-Cre. After 14 days expression, EnvA G-Deleted Rabies-eGFP (Salk Vector Core) was injected to the same coordinates. Following 7 days expression, tissue was harvested, and serial sections were taken throughout the NAc and VP. Starter cells were quantified in the NAcSh, defined as cells-co-expressing mCherry and EGFP; EGFP-positive cells were counted throughout the rostral-caudal extent of the VP using threshold detection function in ImageJ[54].

Perfusion.—Mice were deeply anesthetized with 5% isofluorane and intracardially perfused with 1X phosphate buffered saline (PBS) and then with 4% paraformaldehyde in PBS 1X. Brains were frozen in cooled isopentane (−50°C) and stored at −80°C. Serial coronal or sagittal sections were cut at 40 μm with a cryostat (Leica CM3050) collected in PBS and stored at 4°C.

Imaging.—Slides were initially scanned with an upright fluorescent slide-scanning microscope (Leica DM6 B) at 5X and visualized with Leica Application Suite X software to identify areas of interest. For fluorescent immunohistochemistry experiments, sections were imaged with a confocal laser-scanning microscope (Leica, DMI4000 B) with a 20X air objective. The brightness and contrast of images were adjusted to optimize visualization, and adjustments were applied uniformly across each image. For rabies tracing experiments, 20x images acquired from the Leica slide-scanning microscope; regions of interest were manually delineated based on the atlas of Paxinos and Watson[55], and subsequently imported to ImageJ for cell counting.

Patch Clamp Electrophysiology.

Whole-cell patch-clamp recordings were made from coronal slices (220 μm) of the NAcSh or VP. Slices were prepared using a vibratome (Leica VT 2100) in ice cold cutting solution (in mM: 0,5 $CaCl_2$, 110 $C_5H_{14}CINO$, 25 $C_6H_{12}O_6$, 25 $NaHCO_3$, 7 $MgCl_2$, 11.6 $C_6H_8O_6$, 3.1 $C_3H_3NaO_3$, 2.5 KCl, and 1.25 NaH_2PO_4) and continuously bubbled with 95% O_2 and 5% CO_2. Slices were incubated at 32°C for 30 min in artificial cerebrospinal fluid (aCSF; in mM: 119 NaCl, 2.5 KCl, 1.3 $MgCl_2$, 2.5 $CaCl_2$, 1.0 Na_2HPO_4, 26.2 $NaHCO_3$, and 11 glucose) followed by storage at room temperature until electrophysiological recordings were

performed. Slices were hemisected and superfused with aCSF at 30 ± 2°C. Neurons were recorded using borosilicate glass pipettes (5-7 MΩ resistance) pulled on a micropipette puller (Narishige PC-100) filled with cesium-based internal solution (in mM: 110 CsMeS, 15 KMeS, 0.02 EGTA, 10 Hepes, 0.5 $MgCl_2$, 1.5 $MgSO_4$, 4 ATP-Na_2, 0.3 GTP-Na_3, 10 $C_6H_{12}O_6$, and 10 Phosphocreatine-Na_2 with 7.3 pH and 289 Osm). Currents were amplified, filtered at 2 kHz, and digitized at 10 kHz using a MultiClamp 700B amplifier and Digidata 1550 (Molecular Devices). Clampex 11.4 software (Molecular Devices) was used for data acquisition. Series resistance was monitored by a hyperpolarizing step of −15 mV for 5 msec every 10 sec; the cell was discarded if the series resistance changed by more than 15%. Neurons were visualized using an Olympus 560X upright microscope; field LED illumination (CoolLED) was used to visualize TdTomato or mCherry (560 nm), and stimulate ChR2-expressing terminals (473 nm, paired 4ms light pulses, 50 ms ISI, 13.7-18.2 mW). All agents were purchased from Sigma Biosciences. Coordinates of recorded cells in the NAcSh were captured at 4x on the patch microscope and registered to the atlas of Paxinos and Watson.

In vivo electrophysiology.

Wildtype mice (3M, 3F) were injected with ChR2 in the VP, and 16-channel nickel-coated recording arrays (MWA-250x250-NiCr-50-16-5 -MOD16-1-G2, 50 μm, MicroProbes for Life Science) coupled to an optic fiber (ThorLabs, constructed in house) were implanted in the NAcSh. In an additional 5 wildtype mice (3M, 2F), retrograde Cre was injected in the NAcSh, DIO-ARCH3.0 was injected over the VP. An optic fiber was implanted over the VP and 16-channel recording arrays were implanted in the NAcSh. Neurophysiological signals were transmitted to an Omniplex neurophysiology system (Plexon Inc) via a multiplexing digital headstage, while light was delivered through the optic fiber via a Plexon LED and driver system. Spike channels were acquired at 40 kHz with 16-bit resolution, and band-pass filtered at 150 Hz to 3 kHz before spike sorting. Local field potential signals were simultaneously digitized at 1Khz. Single and multiple units were discriminated using principal component analysis (Offline Sorter; Plexon), using MANCOVA analyses to determine if single unit clusters were statistically distinct from multi-unit clusters. Single units exhibited a mean 2D J3 = 3.41, Daves-Boulin = 0.272, and p value by MANCOVA = 0.00801. Single units were classified into putative MSNs (pMSNs) and putative interneurons (pINs) based on peak-valley duration: pMSNs 462.8 ± 27.96, pINs 242.01 ± 26.27,multi-units 360.1 ± 19.49, CV: pMSNs 1.77 ± 0.25, pINs 1.23 ± 0.17, multi-units 1.49 ± 0.14, Firing Rate: pMSNs 0.40 ± 0.11, pINs 3.53 ± 1.20, multi-units 4.12 ± 0.91. Mice were recorded three times, and the recording with the largest number of channels with unit activity was chosen for analysis. Autocorrelelagrams were performed to exclude duplicate units.

Channelrhodopsin experiments.—To identify light-modulated units, we exported the average peri-event-histogram (PSTH) of spiking of each unit around light onset in 10 msec bins. To test whether a neural response of an isolated NAcSh unit was significantly modulated by activation of local VP terminals, paired t-tests were performed on the average firing activity of each isolated unit in the 50 msec period during light (473 nm). onset relative to activity during the 1 sec baseline period immediately preceding light onset. A unit

was determined to be light-modulated if the difference between the average activity between baseline and light-onset was statistically significant. We used histology and modulation of the LFP by blue light to confirm our recording sites; if there was no significant modulation of LFP by blue light stimulation, units recorded on the same channel were excluded from further analysis (resulted in exclusion of 3 multi - units from 2 mice).

Archaerhodopsin experiments.—Green (550 nm) light was applied to the VP for alternating 40 minute blocks over a 5h recording session during which mice were freely allowed to consume reward. To identify reward-inhibited units for further analysis, we exported the average PSTH of spiking of each unit around reward consumption onset in 10 msec bins. Paired t-tests were performed on the average firing activity of each isolated unit in the 3 sec period preceding lick onset relative to activity during the 1 sec immediately after bout onset. For reward-inhibited units, trials were split according to laser activation. Normalized firing rate for each unit was analyzed with repeated measures ANOVA from the 3 seconds preceding to 5 seconds after reward consumption onset.

Fiber Photometry.

Wildtype mice (13M, 11F) were injected with AAVDJ-hsyn-GCaMP6s-eYFP (NAcSh measurements) or retroAAV-Cre into the NAcSh (vArky measurements, 250 μL, coordinates from bregma: AP: +1.7mm, ML: −0.6mm, DV: −4.5mm). For vArky measurements, AAVDJ-hsyn-DIO-GCaMP6s-eYFP was injected to the VP (300 μL, coordinates from bregma: AP: +0.6mm, ML: −1.5mm, DV: −4.65mm[55]; an additional 9 mice (5M, 4F) were injected with DIO-GFP as controls. An optic fiber (200 μM core, 0.39 numerical aperture, ThorLabs) was implanted unilaterally over the CGaMP injection site and secured with dental cement. Following 3 weeks of viral expression, GCaMP fluorescence was detected through the optic fiber using a fiber photometry system (Neurophotometrics), with all data recorded in Bonsai visual reactive programming language[56]. Photobeam breaks detected with the drinking spout were aligned to the fiber photometry recording using an Arduino Uno as a digital acquisition device (constructed in house), and mice were video-tracked throughout the experiment using Bonsai. Mouse speed was calculated from x y position in NeuroExplorer, and GCaMP signal was aligned to behavioral events. Licking behavior was detected by photo beam breaks. Speed peaks were identified as local maxima in the calculated velocity trace that exceeded 5cm/s. We then scanned backwards in time from this peak in 0.1s bins to identify the first time-point above 2cm/s, which was considered the initiation of the locomotion bout. Locomotor arrests were defined as the 0.1s bin immediately preceding a minimum 2 s period of no change in the x or y position[57]. Permutation analyses were run 2000 times with assignments for high or low trials shuffled before each permutation; the distribution of the resulting differences in lick behavior is shown. Three mice were excluded for optic fiber placements outside the VP.

Head Fixed Intraoral infusion.—Additional wildtype mice were injected with retroAAV-Cre into the NAcSh and AAVDJ-hsyn-DIO-GCaMP6s (4M, 4F) or eYFP (3M, 5F) into the VP, with an optic fiber implanted over the VP as above. Emitted green fluorescence passed through a dichroic (505-535 nm filter, Doric), and was captured with a photodetector (Model 2151, Newport). Analog signals were subsequently amplified and

recorded with a digital acquisiton system (Omniplex, Plexon). Behavioral training was conducted during the dark cycle. Mice were individually allowed to freely drink 5% sucrose, water or 0.05% quinine[58,59] over their dark cycle before having a head post attached in preparation for head restraint. Animals were then habituated to head-fixation on a running wheel for five days, followed by two days of habituation to water infusion via a canulae placed in the mouth. During the experimental sessions, mice received five 20 μL infusions of 5% sucrose, water and 0.05% quinine during fiber photometry recordings. Each infusion last 3 seconds and were performed in a random interval between 1 and 2 minutes. Solutions order were counterbalanced between mice. Fiber photometry recordings were aligned with the infusion start for each trial and data processing was performed as previously described.

Behavioral Assays.

Reward Consumption.—Mice were individually placed in a 30cm x 20cm behavioral arena (Lab Products Rat One Cage 2100™) and given 60 min/day to consume a highly palatable liquid (Nesquik®, Nestlé, Switzerland). The liquid was presented in a liquid feeding tube (Bioserv) in the center of the arena. Before beginning baseline testing, mice were habituated to the behavioral arena for one day.

Baseline testing continued for 9-15 days to ensure habituation. The amount of time the mice spent drinking the liquid was recorded using infrared break-beam sensors connected to a microcontroller (Arduino, Turin, Italy). Following the baseline testing, the mice entered the experimental phase. The experimental phase had three session types: paired stimulation, scrambled stimulation, and no stimulation. In closed-loop stimulation, the drinking behavior was paired with 20 Hz blue light (473 nm) stimulation for the duration of the time spent drinking. In open-loop stimulation, 20 Hz stimulation was delivered randomly throughout the hour-long session. Closed-loop Arch3.0 stimulation occurred under identical conditions, except for the green (515 nm) laser was delivered in a continuous pulse for the duration of the reward bout. The no stimulation sessions were the same as the baseline testing; the mice had optic fibers attached but no stimulation was delivered during that session. The mice were tested for three days for each session type. The order of sessions was counterbalanced between the mice. The amount of time spent drinking and timestamps of each drinking bout were recorded.

Orofacial Taste Reactivity.—Mice were placed individually in a behavioral arena where they had access to a 5% sucrose solution. Tongue protrusions were videotaped at 240 fps and results were manually scored. The first six lick bouts of each sessions was scored over 3 sessions / mouse. Alternating interactions with the sucrose solution were paired with 20 Hz blue light stimulation (473nm), counterbalanced across mice.

Real Time Place Preference.—Mice were individually run in a behavioral arena that had two established zones distinguished by wall patterns. The RTPP was run in three parts: a pretest session, a stimulation session, and a test session. In each session, the mice were attached to optic fibers and placed in the arena for 45 minutes. In the pretest session, the mice freely explored the two zones without any stimulation. In the stimulation session, mice would receive 20 Hz stimulation while in the “active” experimental zone, while there was no

stimulation delivered in the other “inactive” zone. Active and inactive zones were counterbalanced across subjects. The amount of time mice spent in each of the zones was recorded with a USB-powered webcam and zones were detected using Bonsai programing software[56].

Optogenetic ICSS Assay.—Mice were acclimated to behavioral testing chambers equipped with a device composed of two nose pokes, adapted from FED[60,61]. Pokes on the active port resulted in a tone and delivery of 2 seconds of 20 Hz stimulation through the optic fibers, pokes on the inactive nose poke had no effect; the position of the active nosepoke was counterbalanced between subjects. Mice completed 5 daily 60 minute sessions over 5 consecutive days.

Two-Bottle Choice Assay.—Mice were acclimated to an operant chamber equipped with two identical bottles of chocolate milk during their dark cycle[62]. Following this habituation, two identical bottles were again presented but licks registered on one bottle triggered optogenetic stimulation at 20 Hz, 4 ms pulses for the duration of the lick bout, with a minimum duration of 1 sec.

Open Field Test.—Mice were individually run in a behavioral arena (50 cm x 50 cm x 30 cm). Mice were placed in the center of the arena and locomotor activity was recorded for 20 minutes. Afterwards, mice received 20Hz blue light stimulation (473 nm) for 20 minutes while locomotion was recorded. The behavior was recorded with a USB-powered webcam while distance traveled was detected using Bonsai.

Experimental Design and Analysis.

Animals were randomized to treatment groups, except where transgenic lines were required, in which case wildtype littermates were used as matched controls. Data collection and analysis were not performed blind to conditions of the experiment, with the exception of orofacial taste reactivity video scoring. For fiber photometry experiments, 5 mice (2 GCaMP and 3 GFPs) were excluded in the operant task only, due to consistent artefacts from cable bending around pellet retrieval; no other animals were excluded from the analysis. Patch clamp electrophysiology data was analyzed offline in Clampex version 11. In vivo electrophysiological and fiber photometry data were analyzed in NeuroExplorer, to align events to neural activity data. Visualizations and statistics were performed in Python 3.7, or Graphpad Prism version 8. Group sizes were powered to detect effect sizes > 0.2 (Cohen’s d), data met conditions of normality. A p value of 0.05 was considered significant, statistical tests are indicated throughout and were always two-tailed. ANOVA was appropriate repeated measures of mixed-model design was used to test normally distributed data, distributions were compared with two sample Kolmogorov-Smirnov test or Chi-squared tests of two proportions. All data in bar graphs represent mean ± SEM, box and whisker plots indicate mean, and interquartile ranges. Additional details found in the *Life Science Reporting Summary*.

Extended Data

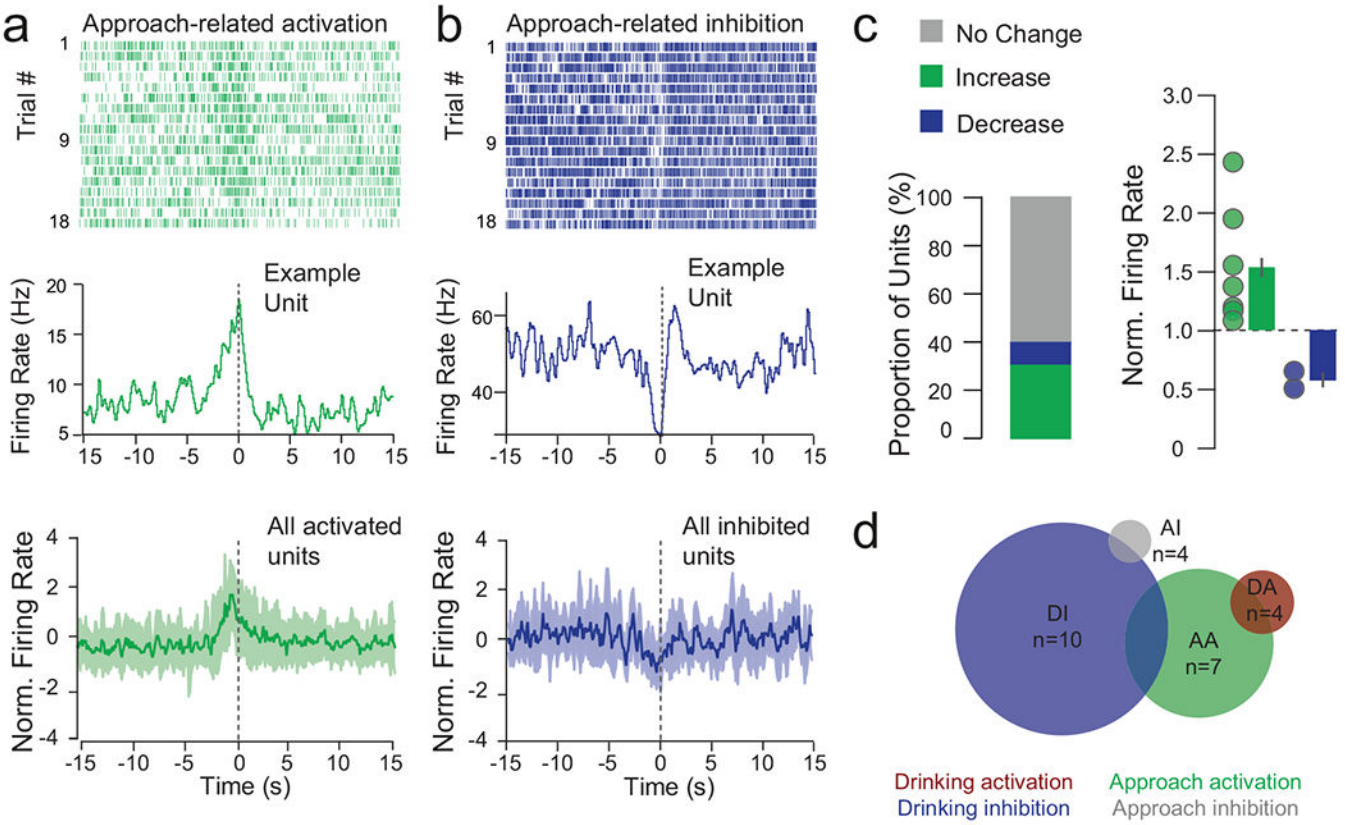

Extended Data Fig. 1. NAcSh units are activated by reward approach.

(a-b) Top: examples of approach-activated and approach-inhibited single units from the same mouse, aligned to drinking onset. Raster and PSTH of units activated and inhibited during reward approach; bottom = mean ± SEM. **(c)** Summary of approach-related responses of n=32 multi-units from 6 mice; 6.25% decrease, 25.0% increase, 68.75% no change, and normalized firing rate changes in response to approach (mean increase = 1.81 ± 0.20, mean decrease = 0.79 ± 0.09; mean ± sem **(d)** Euler diagram showing overlap of functionally defined NAcSh units.

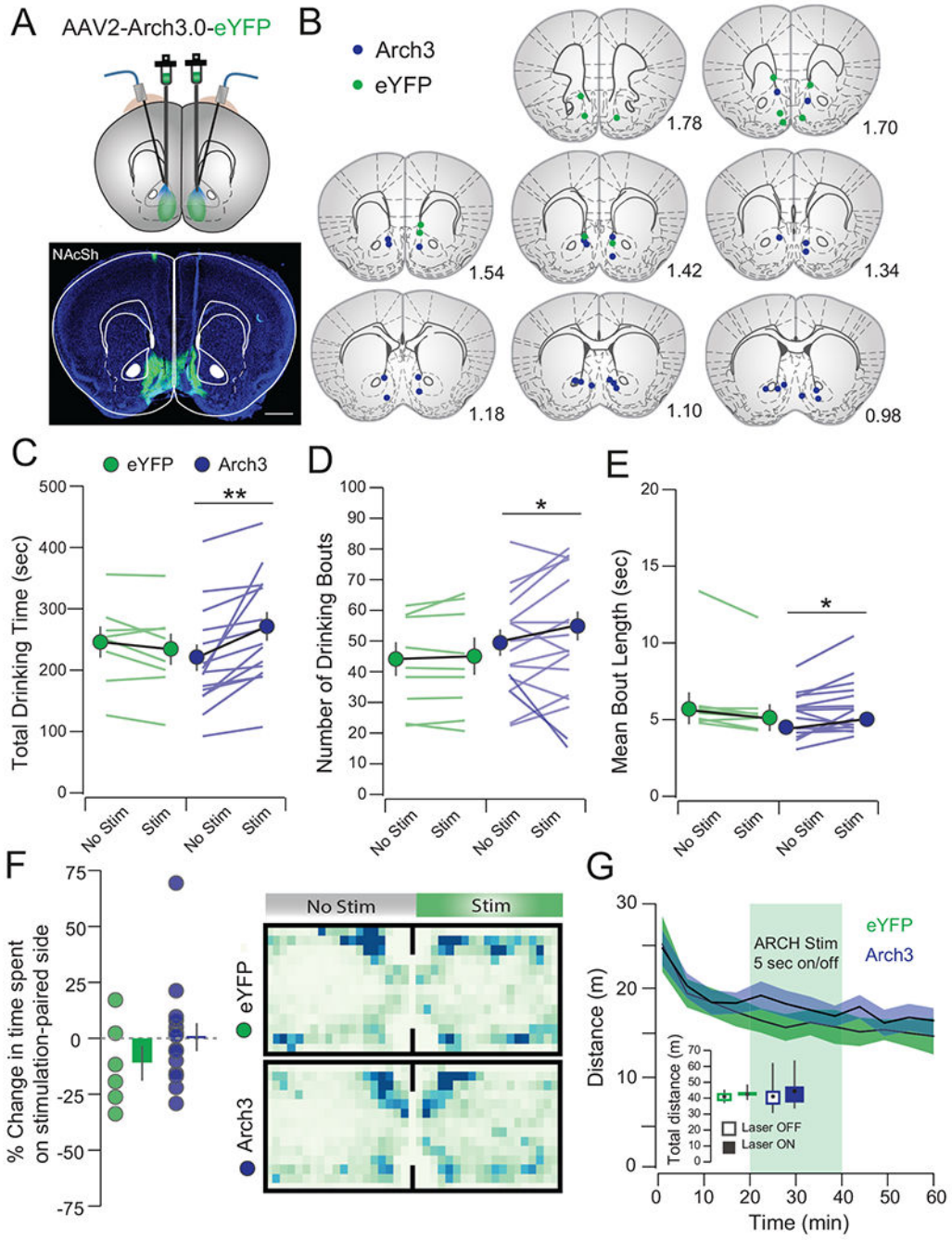

Extended Data Fig. 2. NAcSh inhibition promotes reward consumption without inducing a place preference or locomotor effects.

(a) Histology showing viral infection and optic fiber placement (scale bar = 1 mm). **(b)** Arch stimulation increased total drinking time (Arch No Stim: 217.93±21.57 sec, Arch Stim: 267.95±22.93 sec, $t_{14} = 3.77$, p = 0.002; eYFP No Stim: 24.422±30.03 sec, eYFP Stim: 231.43±25.55 sec, $t_7 = 1.68$, p=0.14), **(c)** number of bouts (Arch No Stim: 48.88±4.29, Arch Stim: 53.63±4.69 sec, $t_{14} = 2.47$, p = 0.038; eYFP No Stim: 43.21±5.40, eYFP Stim: 44.13±6.00, $t_7 = 0.88$, p=0.41) and **(d)** mean bout length (Arch No Stim: 4.63 ± 0.37 sec,

Arch Stim: 5.16±0.46 sec, t_{14} = 2.27, p = 0.040; eYFP No Stim: 5.836 ± 0.847 sec, eYFP Stim:5.836±0.847, t_7 =2.28, p = 0.06). **(e)** Arch3 inhibition did not induce a place preference in a RTPP task (eYFP: −11.92±7.71%, Arch: 1.06±5.96, t_{19}=1.22, p=0.24) or **(f)** alter locomotor activity in an open field task (eYFP No Stim: 320.97±13.41 m, eYFP Stim: 323.41±12.02 m, Arch No Stim: 353.12±22.46 m, Arch Stim: 374.07±21.34 m, $F_{StimxVirus;1,19}$=1.33, p=0.26). n=12/15, eYFP/Arch3). All data is represented as mean ± IQ range. *p<0.05, **p < 0.01

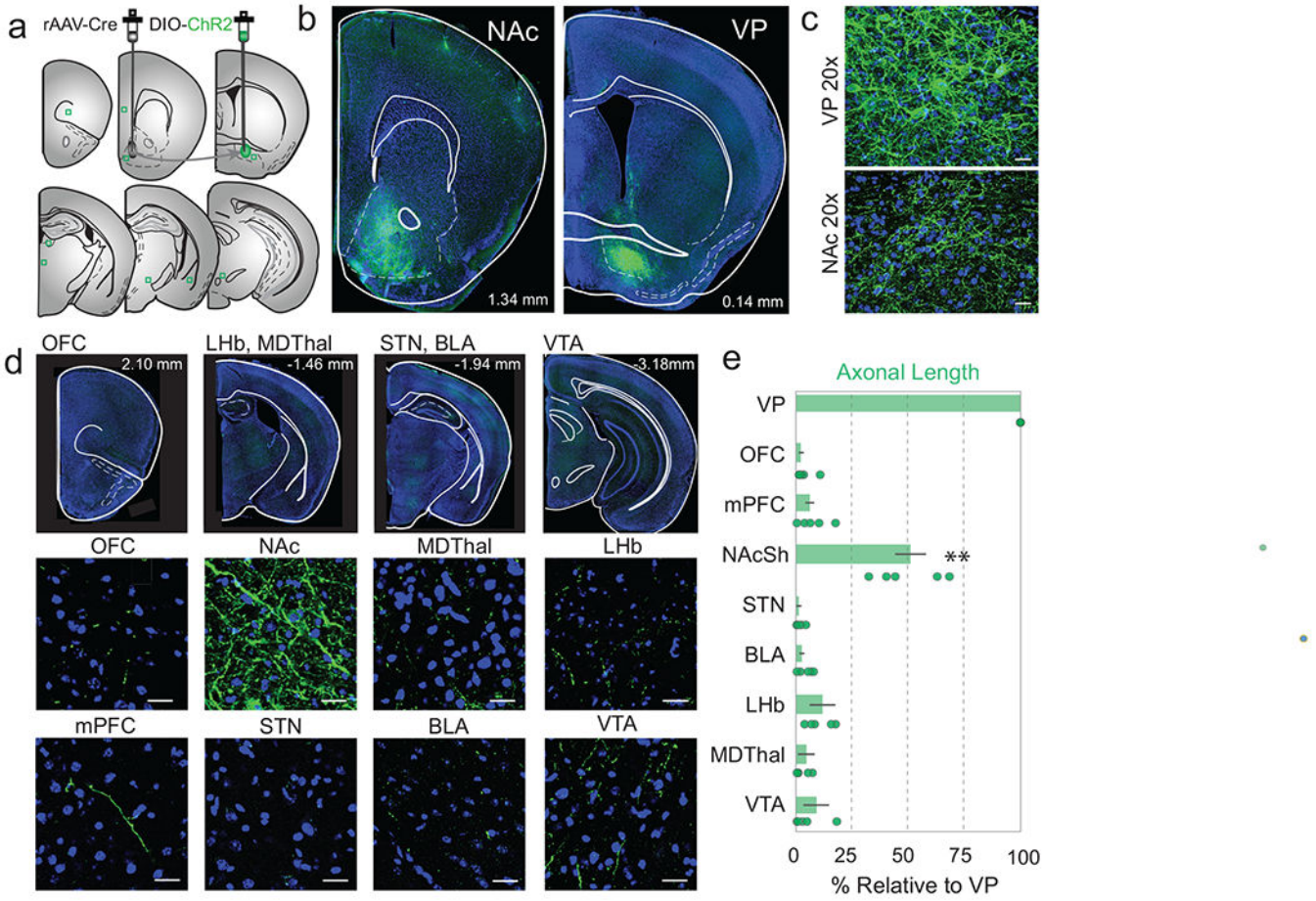

Extended Data Fig. 3. Retrograde viral tracing reveals vArky fibers preferentially in the NAcSh. **(a)** rAAV-Cre was injected in the NAcSh, DIO-ChR2 was injected into the VP and serial sections were taken of known VP projection sites. **(b-c)** 5x and 20x overview of ChR2-labeled terminals in the NAcSh and infected cell bodies in the VP (n=4 sections/brain region, 6 mice). **(d)** 10x representative images of serial sections (top) and 20x confocal images of canonical VP projection areas. **(e)** Quantification of total axonal length, normalized to VP. Intensity and axonal length in the NAcSh was significantly greater than any area examined. Abbreviations: Nucleus accumbens shell (NAcSh), ventral pallidum (VP), medial prefrontal cortex (mPFC), orbitofrontal cortex (OFC), basolateral amygdala (BLA) lateral habenula (LHb), mediodorsal thalamus (MDThal), subthalamic nucleus (STN), ventral tegmental area (VTA). F=148.4 p<0.001, $F_{fluorescence}$=148.4, p = 0.0016 with

Bonferroni correction for multiple comparisons applied. Data presented as mean ± IQ range. Scale bars=25 μm.

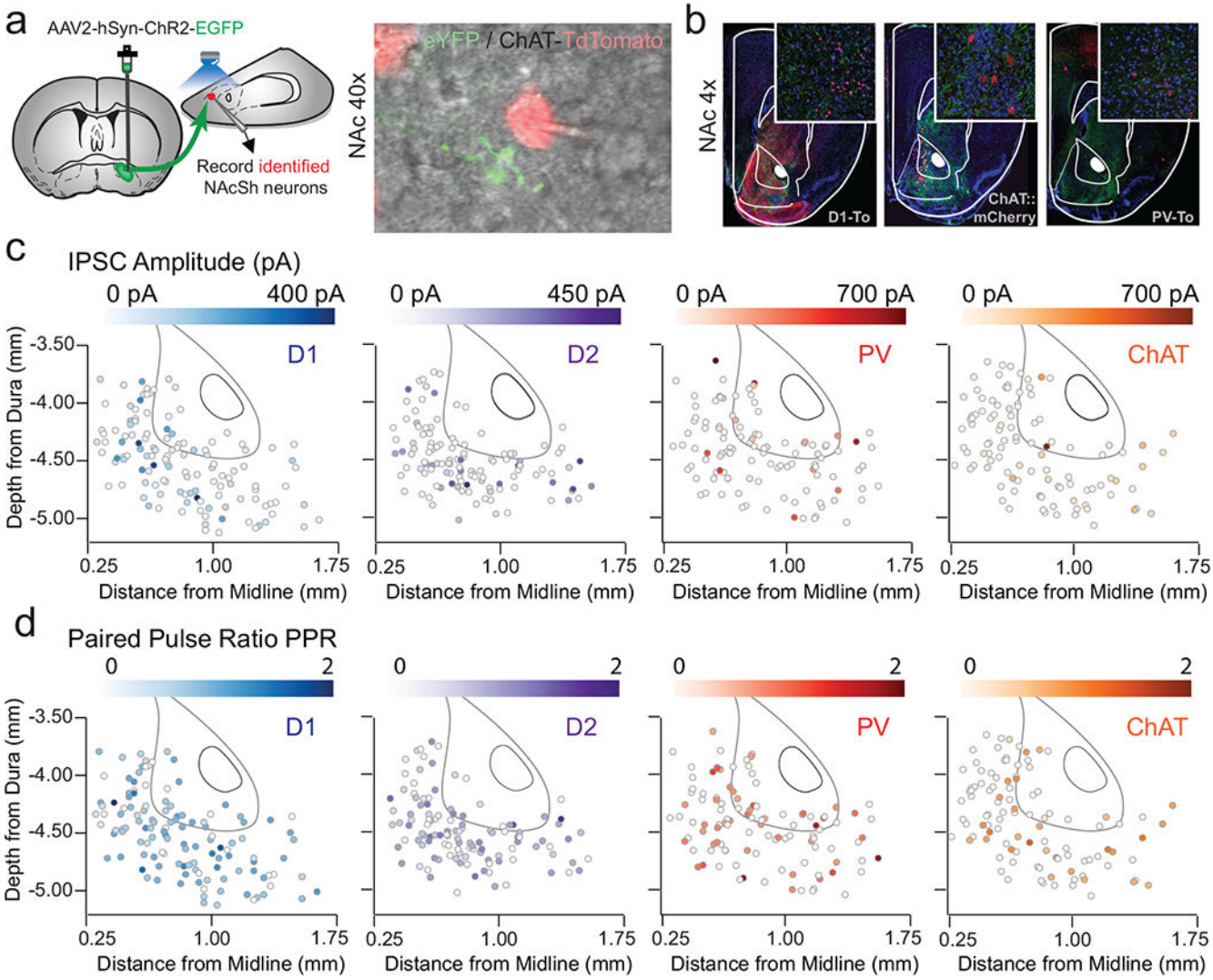

Extended Data Fig. 4. Topography of release properties of VP inputs to NAcSh.

(a) Merged fluorescent image of recorded tomato-expressing neuron adjacent to EYFP-labeled terminals from the VP during patch-clamp experiments. **(b)** 4x image of ChR2-injection site in VP and terminal fields in the NAc in each of three reporter lines. Amplitude **(c)** and PPR **(d)** of oIPSC expressed as location of recorded neuron within the NAcSh in D1-MSNs (n=118 cells / 11 mice), D2-MSNs (n=117 cells / 12 mice), PVs (n=112 cells / 12 mice), and CINs (n=104 cells / 10 mice), scale bar = 50 μM.

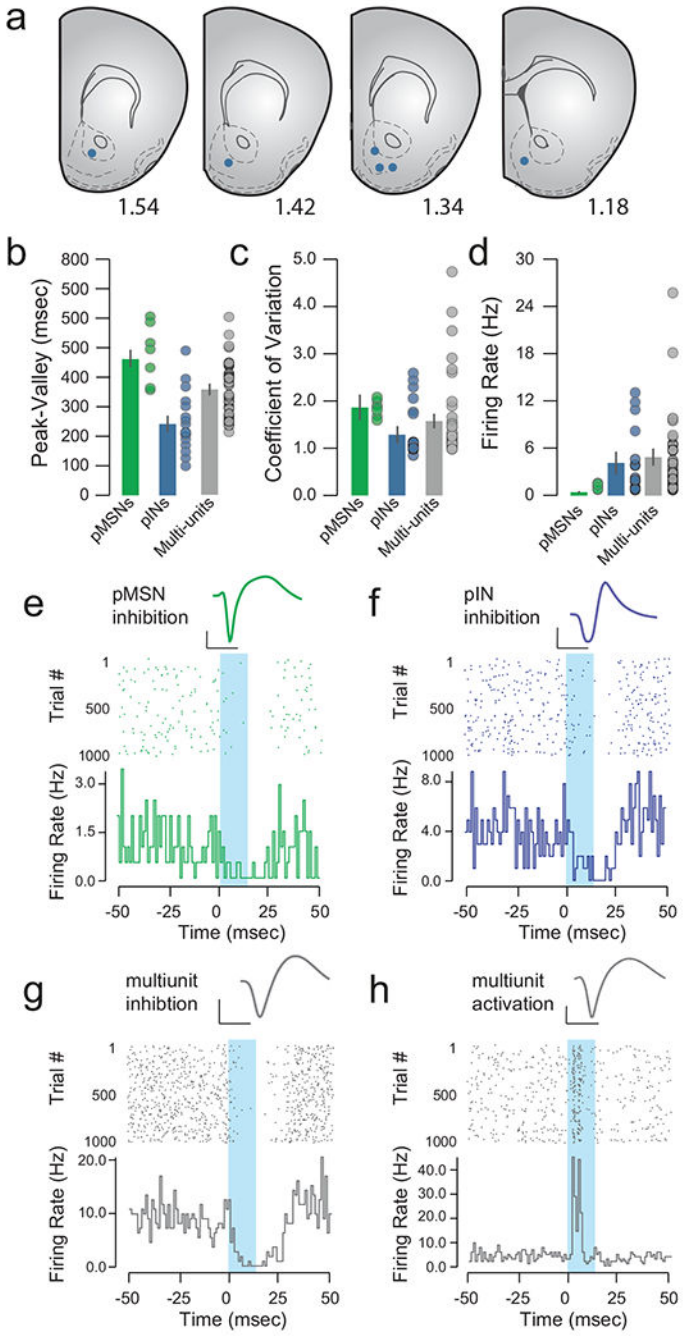

Extended Data Fig. 5. Properties of NAcSh neurons and in vivo responses to activation of vArky terminals.

(a) Location of recording arrays in the NAcSh. **(b-d)** Units were classified according to peak-valley width (n = 9 pMSNs, 14 pINS, 32 multi-units from 6 mice, pMSN: 462.8±27.96 μs, pIN: 242.01±26.27 μs), CV (pMSN: 1.77±0.254, pIN: 1.23±0.17) and firing rate (pMSN: 0.40±0.11 Hz, pIN: 3.53±1.20 Hz, data shown as mean ± IQ range). **(e-h)** representative waveform and PSTH of single neural examples in response to 15 ms of vArky stimulation. Scale bar = 500μs, 50μV.

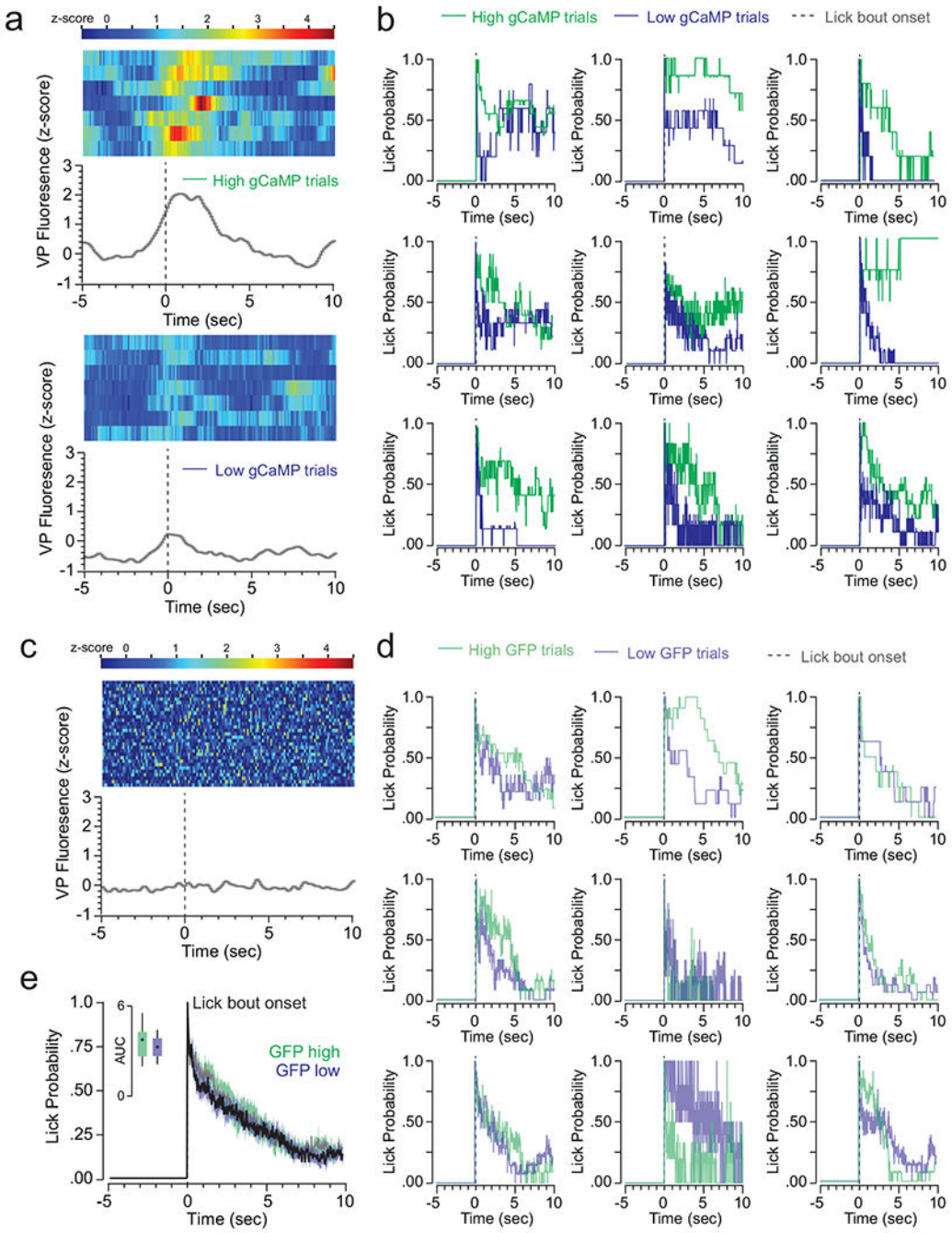

Extended Data Fig. 6. Lick behavior of individual subjects, as a function of high- vs. low-vArky calcium signals.

(a) Single-subject heat map of arkypallidal fluorescence signal across high GCaMP (top) and low GCaMP (bottom) trials aligned to reward consumption onset. **(b)** Lick behavior of high- vs. low-vArky calcium trials of all individual GCaMP-injected subjects. **(c)** Single-subject heat map of fluorescence signal of GFP mouse. **(d)** Lick behavior of high- vs. low-VP signal trials of all GFP-injected subjects, **(e)** Average lick behavior of high and low VP

signal trials of all GFP-injected mice (AUC lick probability high signal trials: 3.16±0.65, AUC lick probability low signal trials: 2.94±0.49, mean ± IQ range).

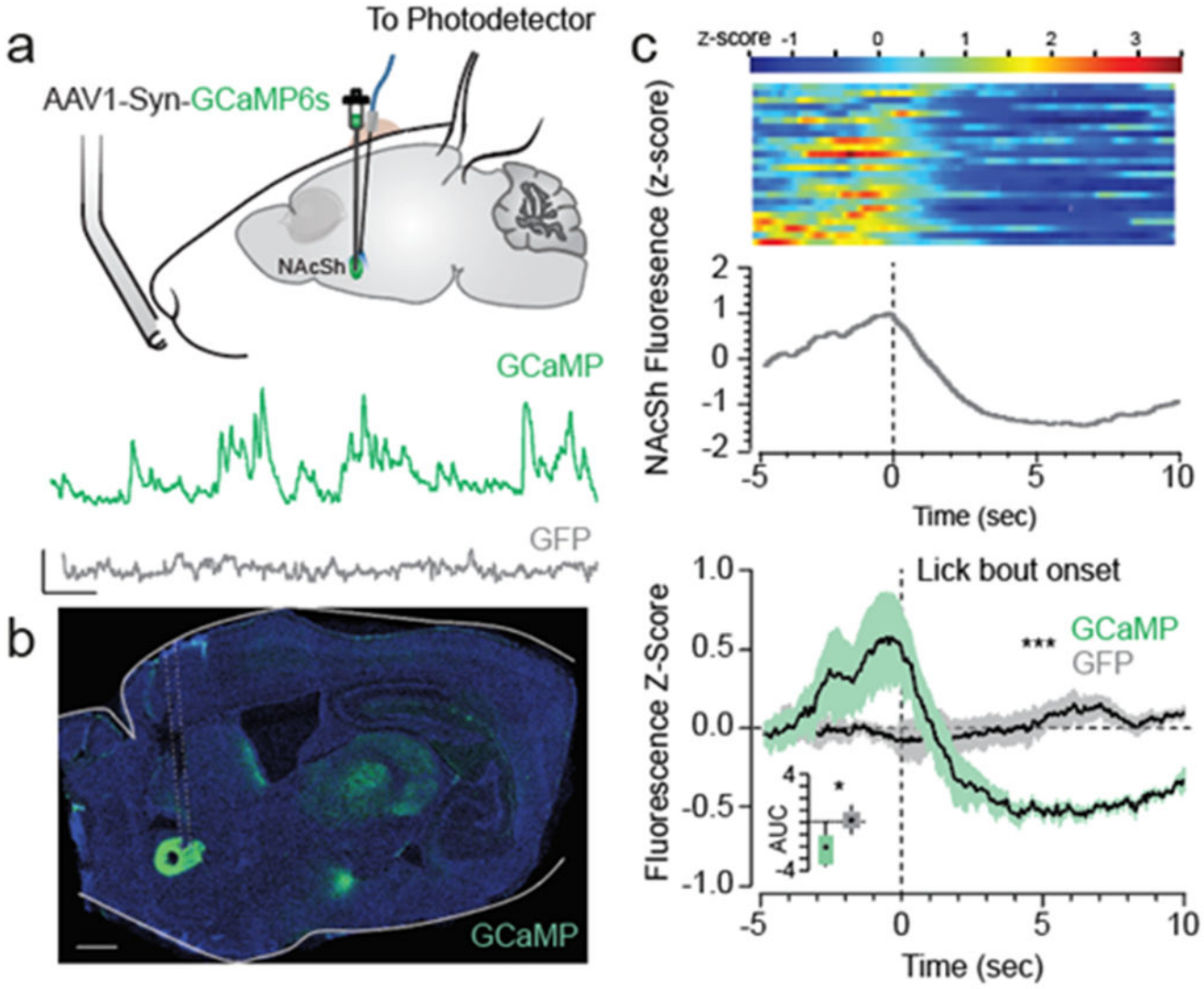

Extended Data Fig. 7. Calcium activity in the NAcSh decreases upon reward consumption onset.
(a-b) GCaMP injection in the NAcSh, representative traces (scale bar: 10 sec, 1 z-score) and histology (n=6/6 GCaMP/GFP mice, scale bar = 1 mm). **(c)** Single-subject heat map of NAcSh GCaMP signal and **(d)** combined signal from all subjects (n=6/6 GCaMP/GFP) aligned to reward consumption onset (mean AUC GCaMP: −2.58±0.65, GFP: −0.14±1.40, t_{11}=2.87, p=0.015, mean ± IQ range).

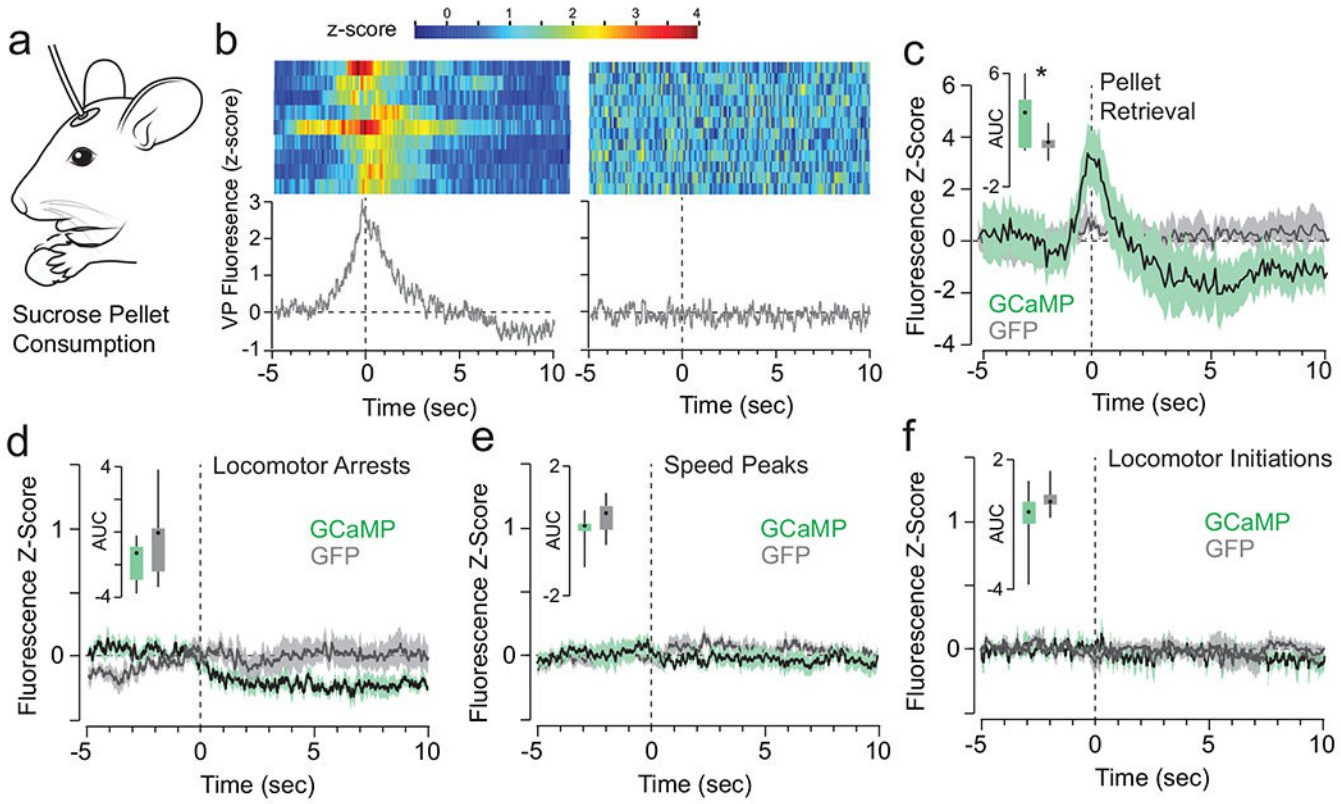

Extended Data Fig. 8. vArky calcium activity increases during sucrose pellet consumption but not locomotor events.

(a) vArky fluorescence signal was recorded during free access consumption of sucrose pellets. **(b)** Representative heat map and normalized calcium signal aligned to sucrose pellet retrieval in GCaMP (left) and GFP (right) expressing mice. **(c)** AUC was significantly greater in the two seconds following pellet retrieval in GCaMP-expressing mice relative to GFP controls (AUC GCAMP: 3.687 ± 0.756, AUC GFP: 0.238 ± 1.378, t_{16}=2.1944, p=0.0433). **(d-f)** Fluorescence responses aligned to locomotor arrests (mean AUC GCaMP: −1.467±0.2994, GFP: −0.3198±1.071, t_{16}=1.127, p=0.27), locomotor initiations (n=704/677 events, AUC GCaMP: −0.818±0.638, GFP: −0.619±1.210, t_{16}=0.150, p=0.88) and peaks in locomotor speed (n=1309/1221 events, mean AUC GCaMP: 0.1294±0.2945, GFP:0.4977±0.3022, t_{16}=0.873, p=0.396). Data mean ± IQ range.

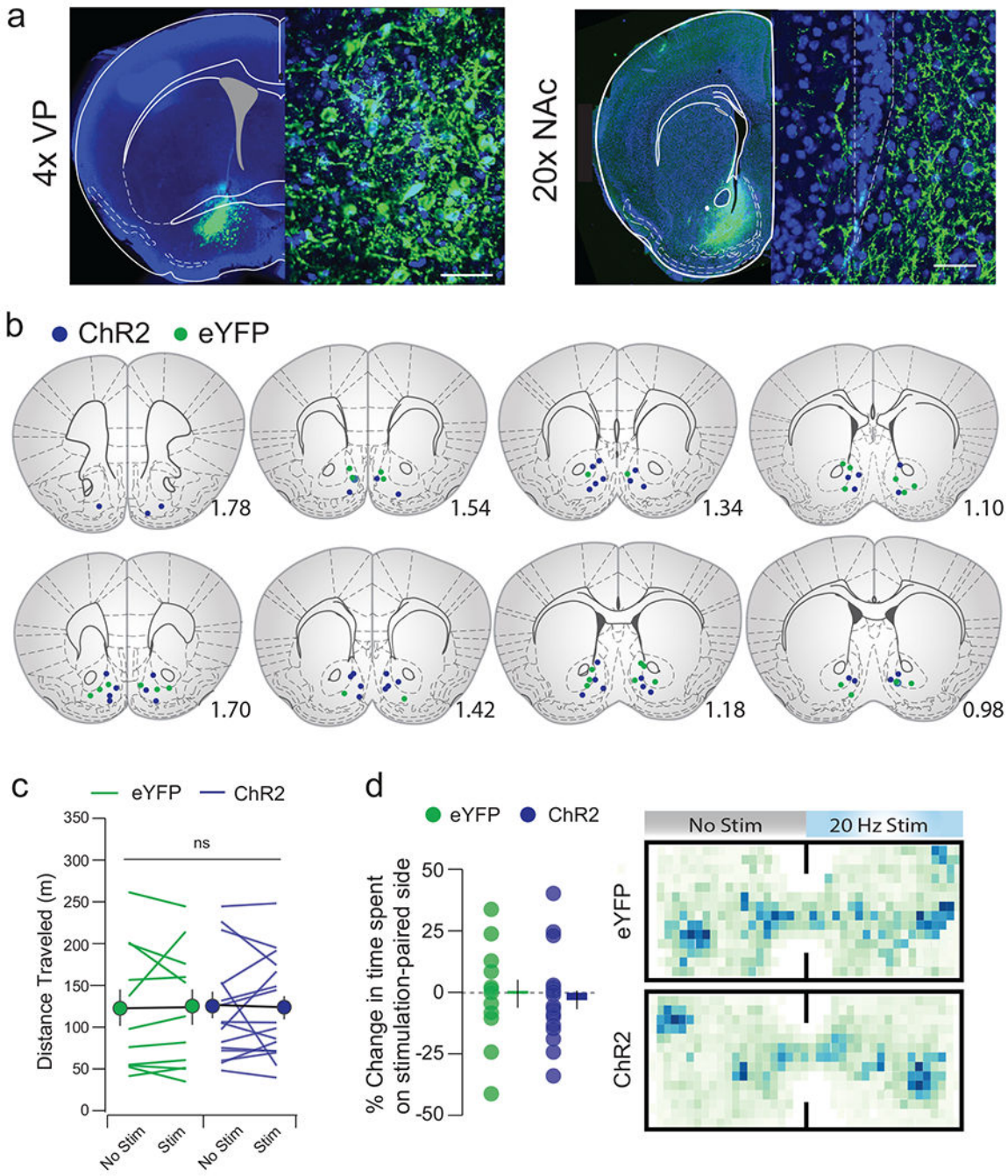

Extended Data Fig. 9. Histological verification, ICSS and RTPP behavioral controls for vArky optogenetic stimulation.

(a) Infection site in VP and terminal fields in NAcSh; scale bar=50μM. **(b)** Verified placements of optic fibers. **(c)** Distance traveled in an open field task (n=12 eYFP, 18 ChR2, eYFPNoStim: 121.62±22.63, eYFPStim : 122.15±21.75, p=0.96, ChR2NoStim: 124.48±16.22, ChR2Stim: 121.83±14.18, Fstim•virus=0.050, p=0.825). **(d)** Preference for the stimulation-paired side of a chamber in a real-time place preference task (n=12 eYFP, 18

ChR2, eYFP: −4.36±4.32%, ChR2: −1.13±5.83) and representative heatmaps. *p<0.05, **p<0.01. All data presented as mean ± sem.

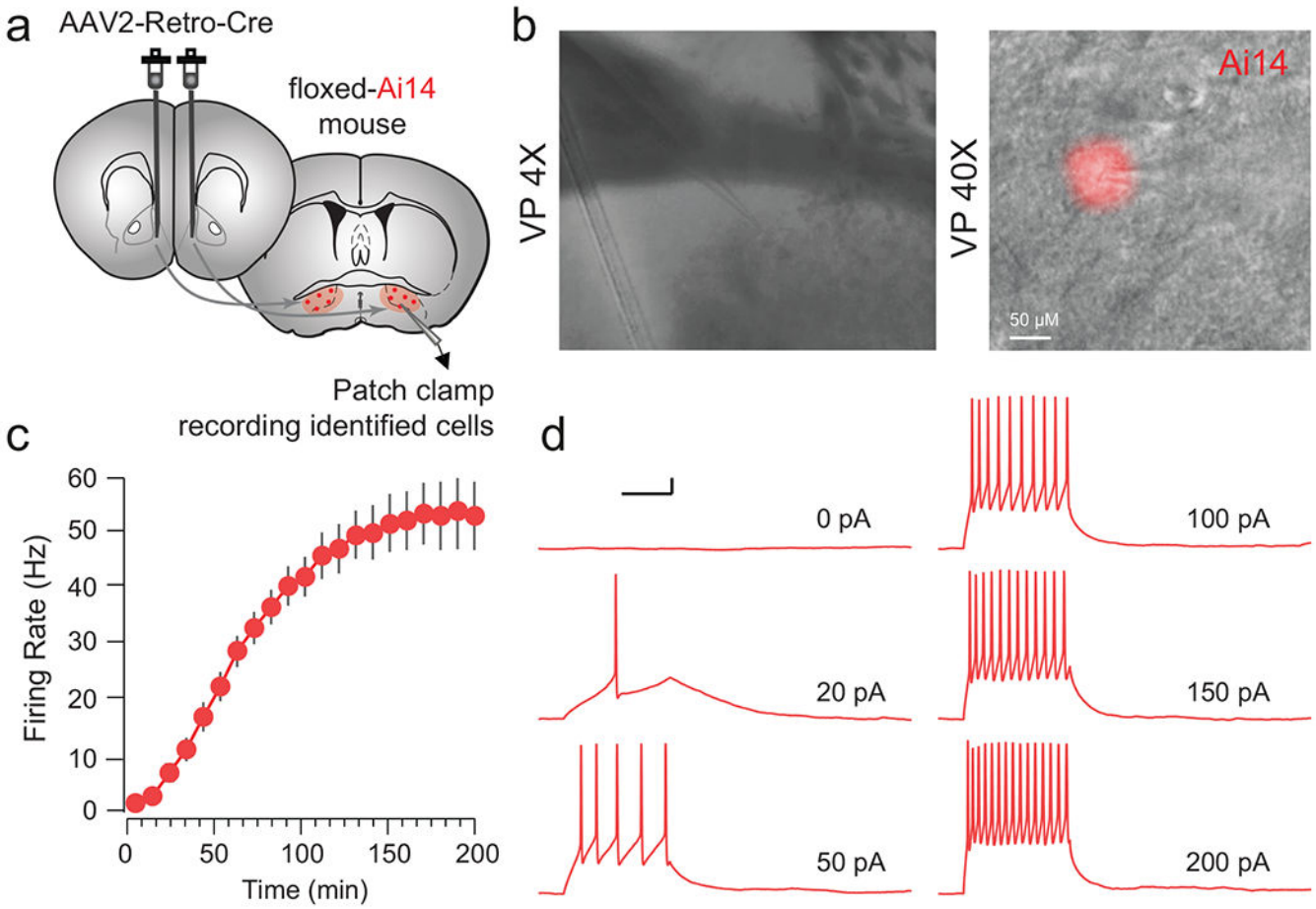

Extended Data Fig. 10. Input-output curves of vArky neuronal responses to current injections ex vivo.

(a) Ai14 reporter mice were injected with retro-cre in the NAcSh to selectively label vArky neurons. **(b)** Merged fluorescent image of Ai14-expressing vArky neurons during patch-clamp experiments (n=12 neurons from 9 mice). **(c)**The mean number of action potentials per second in response to successive current injection (0 to 200 pA) is plotted (error bars: sem). **(d)** Representative traces in response to 50, 100, 150, and 200 pA current injections. Scale bar: 10mV, 100ms.

Supplementary Material

Refer to Web version on PubMed Central for supplementary material.

Acknowledgements:

We thank AV Kravitz for assistance with fiber photometery and in vivo electrophysiology experiments, and MC Stander for excellent technical help. We thank AV Kravitz and I Monosov for critical reading of the manuscript. Graphics used in schematics of experiments were adapted from scidraw.io. Research was supported by the intramural funds from National Institute of Child Health and Human Development (CEL), internal funds from

McDonnell center for systems neuroscience (BMA) and Department of Anesthesiology at Washington University in St. Louis (MCC), the Brain and Behavior Research Foundation (NARSAD Young Investigator Grant #27197 to MCC.), National Institutes of Health National Institute on Drug Abuse (#R21-DA047127, R01-DA049924 to MCC), Whitehall Foundation Grant (#2017-12-54 to MCC.), and Rita Allen Scholar Award in Pain (to MCC.).

References

1. Humphries MD & Prescott TJ The ventral basal ganglia, a selection mechanism at the crossroads of space, strategy, and reward. Prog. Neurobiol 90, 385–417. doi:10.1016/j.pneurobio.2009.11.003 (2010). [PubMed: 19941931]
2. Castro DC & Berridge KC Opioid hedonic hotspot in nucleus accumbens shell: mu, delta, and kappa maps for enhancement of sweetness “liking” and “wanting”. J Neurosci 34, 4239–4250. doi:10.1523/JNEUROSCI.4458-13.2014 (2014). [PubMed: 24647944]
3. Kupchik YM et al. Coding the direct/indirect pathways by D1 and D2 receptors is not valid for accumbens projections. Nat. Neurosci 18, 1230–1232. doi:10.1038/nn.4068 (2015). [PubMed: 26214370]
4. Creed M, Ntamati NR, Chandra R, Lobo MK & Lüscher C Convergence of reinforcing and anhedonic cocaine effects in the ventral pallidum. Neuron 92, 214–226. doi:10.1016/j.neuron.2016.09.001 (2016). [PubMed: 27667004]
5. Williams DJ, Crossman AR & Slater P The efferent projections of the nucleus accumbens in the rat. Brain Res 130, 217–227. doi:10.1016/0006-8993(77)90271-2 (1977). [PubMed: 884524]
6. Krause M, German PW, Taha SA & Fields HL A pause in nucleus accumbens neuron firing is required to initiate and maintain feeding. J. Neurosci 30, 4746–4756. doi:10.1523/JNEUROSCI.0197-10.2010 (2010a). [PubMed: 20357125]
7. O’Connor EC et al. Accumbal D1R neurons projecting to lateral hypothalamus authorize feeding. Neuron 88, 553–564. doi:10.1016/j.neuron.2015.09.038 (2015). [PubMed: 26593092]
8. Roitman MF, Wheeler RA & Carelli RM Nucleus accumbens neurons are innately tuned for rewarding and aversive taste stimuli, encode their predictors, and are linked to motor output. Neuron 45, 587–597. doi:10.1016/j.neuron.2004.12.055 (2005). [PubMed: 15721244]
9. Faure A, Richard JM & Berridge KC Desire and dread from the nucleus accumbens: cortical glutamate and subcortical GABA differentially generate motivation and hedonic impact in the rat. PLoS ONE 5, e11223. doi:10.1371/journal.pone.0011223 (2010). [PubMed: 20585461]
10. Stratford TR Activation of feeding-related neural circuitry after unilateral injections of muscimol into the nucleus accumbens shell. Brain Res 1048, 241–250. doi:10.1016/j.brainres.2005.05.002 (2005a). [PubMed: 15921658]
11. Brog JS, Salyapongse A, Deutch AY & Zahm DS The patterns of afferent innervation of the core and shell in the “accumbens” part of the rat ventral striatum: immunohistochemical detection of retrogradely transported fluoro-gold. J. Comp. Neurol 338, 255–278. doi:10.1002/cne.903380209 (1993). [PubMed: 8308171]
12. Churchill L & Kalivas PW A topographically organized gamma-aminobutyric acid projection from the ventral pallidum to the nucleus accumbens in the rat. J. Comp. Neurol 345, 579–595. doi:10.1002/cne.903450408 (1994). [PubMed: 7962701]
13. Spooren WP, Lynd-Balta E, Mitchell S & Haber SN Ventral pallidostriatal pathway in the monkey: evidence for modulation of basal ganglia circuits. J. Comp. Neurol 370, 295–312. doi:10.1002/(SICI)1096-9861(19960701)370:3<295::AID-CNE2>3.0.CO;2-# (1996). [PubMed: 8799857]
14. Mallet N et al. Dichotomous organization of the external globus pallidus. Neuron 74, 1075–1086. doi:10.1016/j.neuron.2012.04.027 (2012). [PubMed: 22726837]
15. Mallet N et al. Arkypallidal cells send a stop signal to striatum. Neuron 89, 308–316. doi:10.1016/j.neuron.2015.12.017 (2016). [PubMed: 26777273]
16. Glajch KE et al. Npas1+ pallidal neurons target striatal projection neurons. J. Neurosci 36, 5472–5488. doi:10.1523/JNEUROSCI.1720-15.2016 (2016). [PubMed: 27194328]
17. Ambroggi F, Ghazizadeh A, Nicola SM & Fields HL Roles of nucleus accumbens core and shell in incentive-cue responding and behavioral inhibition. J. Neurosci 31, 6820–6830. doi:10.1523/JNEUROSCI.6491-10.2011 (2011). [PubMed: 21543612]

18. Richard JM, Ambroggi F, Janak PH & Fields HL Ventral pallidum neurons encode incentive value and promote cue-elicited instrumental actions. Neuron 90, 1165–1173. doi:10.1016/j.neuron.2016.04.037 (2016). [PubMed: 27238868]
19. Ottenheimer D, Richard JM & Janak PH Ventral pallidum encodes relative reward value earlier and more robustly than nucleus accumbens. Nat Commun 9, 4350. doi:10.1038/s41467-018-06849-z (2018). [PubMed: 30341305]
20. Fujimoto A et al. Signaling incentive and drive in the primate ventral pallidum for motivational control of goal-directed action. J Neurosci 39, 1793–1804. doi:10.1523/JNEUROSCI.2399-18.2018 (2019). [PubMed: 30626695]
21. White JK et al. A neural network for information seeking. Nat Commun 10, 5168. doi:10.1038/s41467-019-13135-z (2019). [PubMed: 31727893]
22. Cheer JF, Heien MLAV, Garris PA, Carelli RM & Wightman RM Simultaneous dopamine and single-unit recordings reveal accumbens GABAergic responses: implications for intracranial self-stimulation. Proc. Natl. Acad. Sci. U.S.A 102, 19150–19155. doi:10.1073/pnas.0509607102 (2005). [PubMed: 16380429]
23. Taha SA & Fields HL Encoding of palatability and appetitive behaviors by distinct neuronal populations in the nucleus accumbens. J. Neurosci 25, 1193–1202. doi:10.1523/JNEUROSCI.3975-04.2005 (2005). [PubMed: 15689556]
24. Taha SA & Fields HL Inhibitions of nucleus accumbens neurons encode a gating signal for reward-directed behavior. J. Neurosci 26, 217–222. doi:10.1523/JNEUROSCI.3227-05.2006 (2006). [PubMed: 16399690]
25. Roitman MF, Wheeler RA, Tiesinga PHE, Roitman JD & Carelli RM Hedonic and nucleus accumbens neural responses to a natural reward are regulated by aversive conditioning. Learn. Mem 17, 539–546. doi:10.1101/lm.1869710 (2010). [PubMed: 20971936]
26. Tachibana Y & Hikosaka O The primate ventral pallidum encodes expected reward value and regulates motor action. Neuron 76, 826–837. doi:10.1016/j.neuron.2012.09.030 (2012). [PubMed: 23177966]
27. Ledbetter NM, Chen CD & Monosov IE Multiple mechanisms for processing reward uncertainty in the primate basal forebrain. J. Neurosci 36, 7852–7864. doi:10.1523/JNEUROSCI.1123-16.2016 (2016). [PubMed: 27466331]
28. Faget L et al. Opponent control of behavioral reinforcement by inhibitory and excitatory projections from the ventral pallidum. Nat Commun 9, 849. doi:10.1038/s41467-018-03125-y (2018). [PubMed: 29487284]
29. Tooley J et al. Glutamatergic Ventral Pallidal Neurons Modulate Activity of the Habenula-Tegmental Circuitry and Constrain Reward Seeking. Biol. Psychiatry 83, 1012–1023. doi:10.1016/j.biopsych.2018.01.003 (2018). [PubMed: 29452828]
30. Berridge KC Measuring hedonic impact in animals and infants: microstructure of affective taste reactivity patterns. Neurosci Biobehav Rev 24, 173–198. doi:10.1016/s0149-7634(99)00072-x (2000a). [PubMed: 10714382]
31. Strickland JA, Austen JM & Sanderson DJ A biphasic reduction in a measure of palatability following sucrose consumption in mice. Physiol. Behav 184, 129–134. doi:10.1016/j.physbeh.2017.11.019 (2018). [PubMed: 29155248]
32. Adamantidis AR et al. Optogenetic interrogation of dopaminergic modulation of the multiple phases of reward-seeking behavior. J Neurosci 31, 10829–10835. doi:10.1523/JNEUROSCI.2246-11.2011 (2011). [PubMed: 21795535]
33. Witten IB et al. Recombinase-driver rat lines: tools, techniques, and optogenetic application to dopamine-mediated reinforcement. Neuron 72, 721–733. doi:10.1016/j.neuron.2011.10.028 (2011). [PubMed: 22153370]
34. Leung BK & Balleine BW The ventral striato-pallidal pathway mediates the effect of predictive learning on choice between goal-directed actions. J Neurosci 33, 13848–13860. doi:10.1523/JNEUROSCI.1697-13.2013 (2013). [PubMed: 23966704]
35. Chang SE, Todd TP & Smith KS Paradoxical accentuation of motivation following accumbens-pallidum disconnection. Neurobiol Learn Mem 149, 39–45. doi:10.1016/j.nlm.2018.02.001 (2018). [PubMed: 29408054]

36. Peciña S & Berridge KC Hedonic hot spot in nucleus accumbens shell: where do mu-opioids cause increased hedonic impact of sweetness? J Neurosci 25, 11777–11786. doi:10.1523/JNEUROSCI.2329-05.2005 (2005). [PubMed: 16354936]
37. Brown MTC et al. Ventral tegmental area GABA projections pause accumbal cholinergic interneurons to enhance associative learning. Nature 492, 452–456. doi:10.1038/nature11657 (2012). [PubMed: 23178810]
38. Collins AL et al. Nucleus accumbens cholinergic interneurons oppose cue-motivated behavior. Biol Psychiatry 86, 388–396. doi:10.1016/j.biopsych.2019.02.014 (2019). [PubMed: 30955842]
39. Reynolds SM & Berridge KC Glutamate motivational ensembles in nucleus accumbens: rostrocaudal shell gradients of fear and feeding. Eur. J. Neurosci 17, 2187–2200. doi:10.1046/j.1460-9568.2003.02642.x (2003). [PubMed: 12786986]
40. Reed SJ et al. Coordinated Reductions in excitatory input to the nucleus accumbens underlie food consumption. Neuron 99, 1260–1273.e4. doi:10.1016/j.neuron.2018.07.051 (2018). [PubMed: 30146308]
41. Richard JM, Plawecki AM & Berridge KC Nucleus accumbens GABAergic inhibition generates intense eating and fear that resists environmental retuning and needs no local dopamine. Eur. J. Neurosci 37, 1789–1802. doi:10.1111/ejn.12194 (2013). [PubMed: 23551138]
42. Van Bockstaele EJ & Pickel VM GABA-containing neurons in the ventral tegmental area project to the nucleus accumbens in rat brain. Brain Res 682, 215–221. doi:10.1016/0006-8993(95)00334-m (1995). [PubMed: 7552315]
43. Hurley SW & Johnson AK The role of the lateral hypothalamus and orexin in ingestive behavior: a model for the translation of past experience and sensed deficits into motivated behaviors. Front Syst Neurosci 8, 216. doi:10.3389/fnsys.2014.00216 (2014). [PubMed: 25431553]
44. Wakabayashi KT et al. Chemogenetic activation of ventral tegmental area GABA neurons, but not mesoaccumbal GABA terminals, disrupts responding to reward-predictive cues. Neuropsychopharmacology 44, 372–380. doi:10.1038/s41386-018-0097-6 (2019). [PubMed: 29875446]
45. van Zessen R, Phillips JL, Budygin EA & Stuber GD Activation of VTA GABA neurons disrupts reward consumption. Neuron 73, 1184–1194. doi:10.1016/j.neuron.2012.02.016 (2012). [PubMed: 22445345]
46. Jennings JH et al. Visualizing hypothalamic network dynamics for appetitive and consummatory behaviors. Cell 160, 516–527. doi:10.1016/j.cell.2014.12.026 (2015). [PubMed: 25635459]
47. Marino RAM et al. Control of food approach and eating by a GABAergic projection from lateral hypothalamus to dorsal pons. Proc Natl Acad Sci U.S.A 117, 8611–8615. doi:10.1073/pnas.1909340117 (2020). [PubMed: 32229573]
48. Root DH et al. Slow phasic and tonic activity of ventral pallidal neurons during cocaine self-administration. Synapse 66, 106–127. doi:10.1002/syn.20990 (2012). [PubMed: 21953543]
49. Ottenheimer DJ et al. A quantitative reward prediction error signal in the ventral pallidum. Nat Neurosci. 23, 1267–1276. doi:10.1038/s41593-020-0688-5 (2020). [PubMed: 32778791]
50. Bocklisch C et al. Cocaine disinhibits dopamine neurons by potentiation of GABA transmission in the ventral tegmental area. Science 341, 1521–1525. doi:10.1126/science.1237059 (2013). [PubMed: 24072923]

Methods-only References:

51. Alpizar SA, Baker AL, Gulledge AT & Hoppa MB Loss of neurofascin-186 disrupts alignment of ankyrinG relative to its binding partners in the axon initial segment. Front Cell Neurosci. 13, 1. doi: 10.3389/fncel.2019.00001 (2019). [PubMed: 30723396]
52. Renier N et al. Mapping of brain activity by automated volume analysis of immediate early genes. Cell 165, 1789–1802. doi:10.1016/j.cell.2016.05.007 (2016). [PubMed: 27238021]
53. Renier N et al. iDISCO: a simple, rapid method to immunolabel large tissue samples for volume imaging. Cell 159, 896–910. doi:10.1016/j.cell.2014.10.010 (2014). [PubMed: 25417164]
54. Schindelin J et al. Fiji: an open-source platform for biological-image analysis. Nat. Methods 9, 676–682. doi:10.1038/nmeth.2019 (2012). [PubMed: 22743772]

55. Paxinos G & Franklin BJF The Mouse Brain in Stereotaxic Coordinates Compact Fifth Edition (Academic, San Diego, 2019).

56. Lopes G et al. Bonsai: an event-based framework for processing and controlling data streams. Front Neuroinform 9, 7. doi:10.3389/fninf.2015.00007 (2015). [PubMed: 25904861]

57. Fobbs WC et al. Continuous representations of speed by striatal medium spiny neurons. J. Neurosci doi:10.1523/JNEUROSCI.1407-19.2020 (2020).

58. Parker LA Aversive taste reactivity: reactivity to quinine predicts aversive reactivity to lithium-paired sucrose solution. Pharmacol Biochem Behav 47, 73–75. doi:10.1016/0091-3057(94)90113-9 (1994). [PubMed: 8115431]

59. Berridge KC Measuring hedonic impact in animals and infants: microstructure of affective taste reactivity patterns. Neurosci Biobehav Rev 24, 173–198. doi:10.1016/s0149-7634(99)00072-x (2000a). [PubMed: 10714382]

60. Nguyen KP et al. Feeding Experimentation Device (FED): Construction and Validation of an Open-source Device for Measuring Food Intake in Rodents. United States. (2017).

61. Nguyen KP, O'Neal TJ, Bolonduro OA, White E & Kravitz AV Feeding Experimentation Device (FED): A flexible open-source device for measuring feeding behavior. J Neurosci Methods 267, 108–114. doi:10.1016/j.jneumeth.2016.04.003 (2016). [PubMed: 27060385]

62. Godynyuk E, Bluitt MN, Tooley JR, Kravitz AV & Creed MC An Open-Source, Automated Home-Cage Sipper Device for Monitoring Liquid Ingestive Behavior in Rodents. eNeuro 6. doi:10.1523/ENEURO.0292-19.2019 (2019).

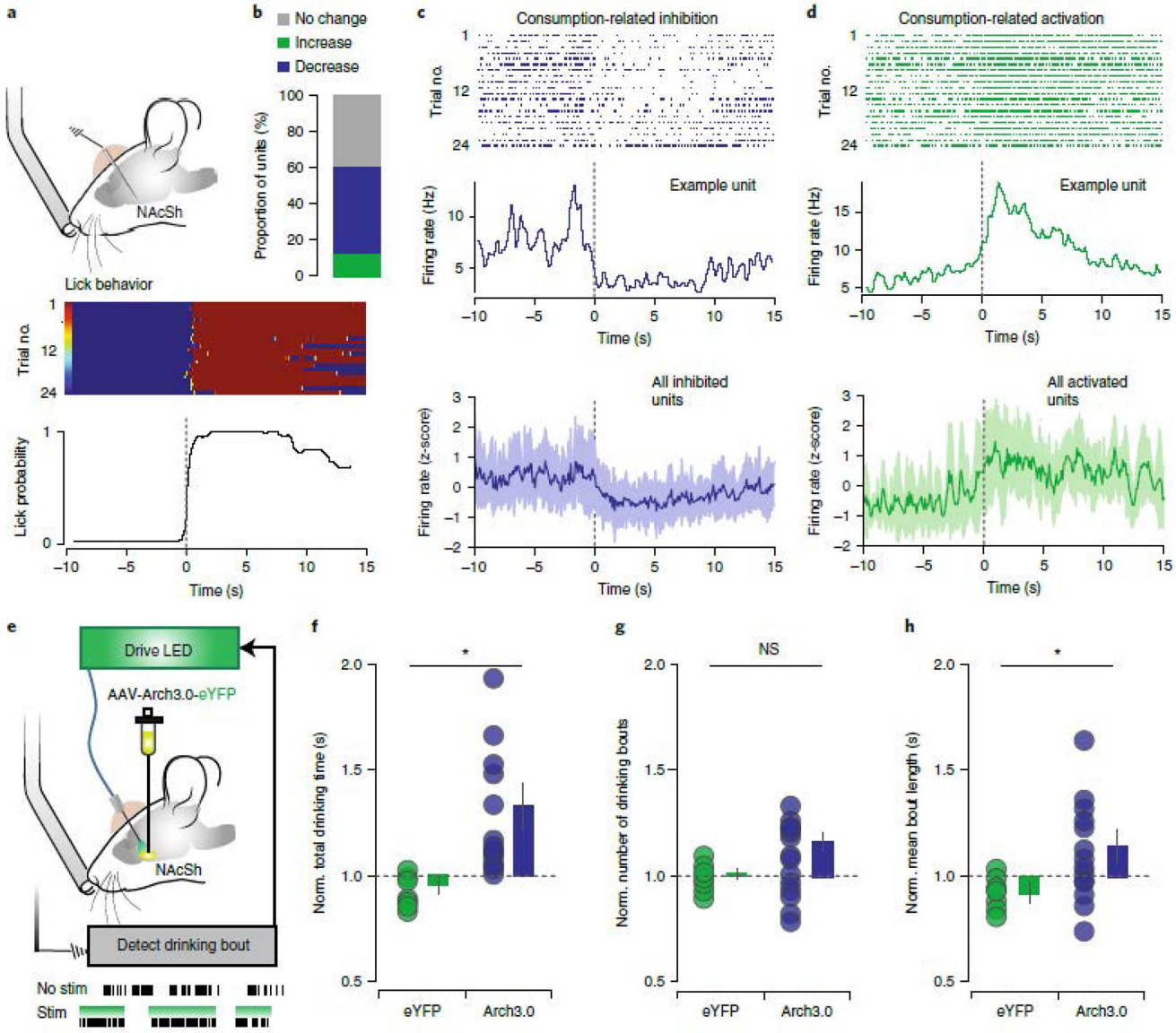

Figure 1. NAcSh inhibition is causally related to reward consumption.

(a) In vivo recording of the NAcSh during free-access paradigm (n=32 multi-units, 6 mice). **(b)** Summary of drinking-related responses of NAcSh units; 35.71% decrease, 10.71% increase, 53.57% no change. **(c-d)** Top: examples of reward-inhibited and reward-activated single units from the same mouse, aligned to drinking onset. Raster and PSTH of units inhibited (C) and activated (D) during reward consumption; bottom = mean ± SEM. **(e)** Closed-loop optogenetic inhibition of NAcSh neurons during reward consumption (n=12/15 eYFP/Arch3). **(f-h)** Optogenetic inhibition increased total drinking time (Arch: 1.29 ± 0.11, eYFP: 0.95 ± 0.03; $F = 9.97$, $p = 0.005$), number of drinking bouts (Arch: 1.01 ± 0.02, eYFP: 1.16 ± 0.06; $F = 3.13$, $p = 0.091$) and bout length (Arch: 1.12 ± 0.06, eYFP: 0.93 ± 0.02; $F = 5.78$, $p = 0.026$) relative to eYFP controls. mean ± SEM * $p < 0.05$

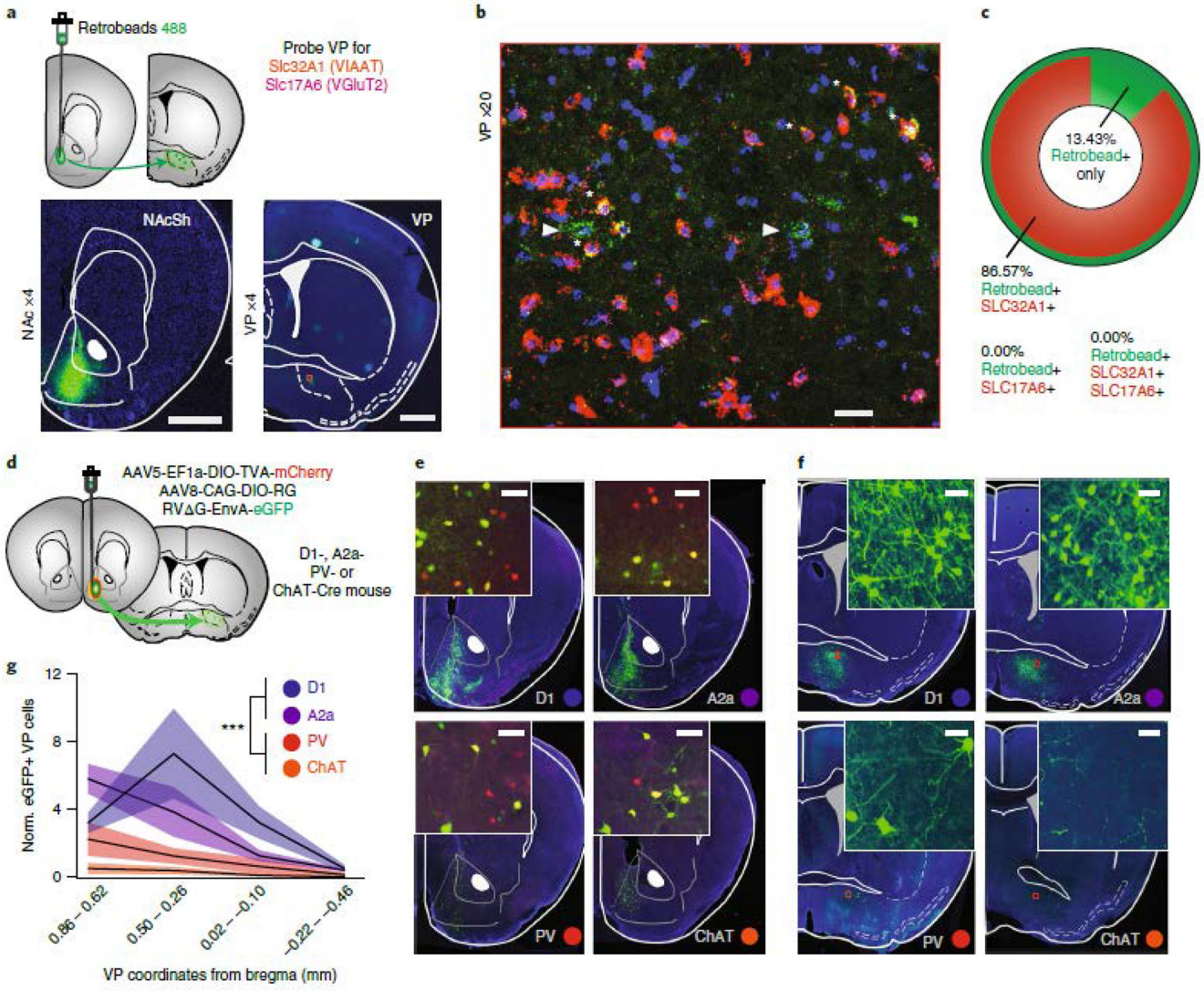

Figure 2. A subpopulation of VP neurons innervates projection and interneurons in the NAcSh.

(a) Green retrobeads were injected in the NAcSh, VP sections were probed for VIAAT (555 nm, red) and VGluT2 (647 nm; magenta) using fISH (n= 15 sections / 3 mice, scale bar = 1mm). **(b)** Representative 20x confocal image showing green-labelled retrobeads in the VP co-localized with VIAAT, scale bar = 25 μM. **(c)** Quantification of overlap between retrobeads and VIAAT (86.57% of retrobead+ neurons) and VGluT2 (0%, no co-localization). **(d)** Schematic of rabies tracing viral injection strategy. **(e)** Representative images of injection sites in NAcSh in D1-Cre (n = 5 mice), A2a-Cre (n = 5 mice), PV-Cre (n = 5 mice) and ChAT-Cre (n = 7) mice; inset = 20x confocal images showing starter cells (scale bar = 50 μM). **(f)** Representative images of EGFP-infected projection neurons in the VP; inset = 20x confocal images (scale bar = 50 μM). **(g)** Quantification of the number of EGFP+ VP cells, normalized to number of starter cells in the NAcSh is expressed across the anterior-posterior VP gradient revealed a significant effect of genotype, with D1- and A2a-Cre mice exhibiting denser labelling than PV-Cre or ChAT-Cre mice ($F_{15} = 13.56$, $p<0.001$,

D1-Cre = 3.67 ± 0.79, A2a-Cre = 3.50 ± 0.81, PV-Cre = 1.07 ± 0.37, ChAT-Cre = 0.25 ± 0.10 EGFP+ive cells/starter cell, mean ± sem).

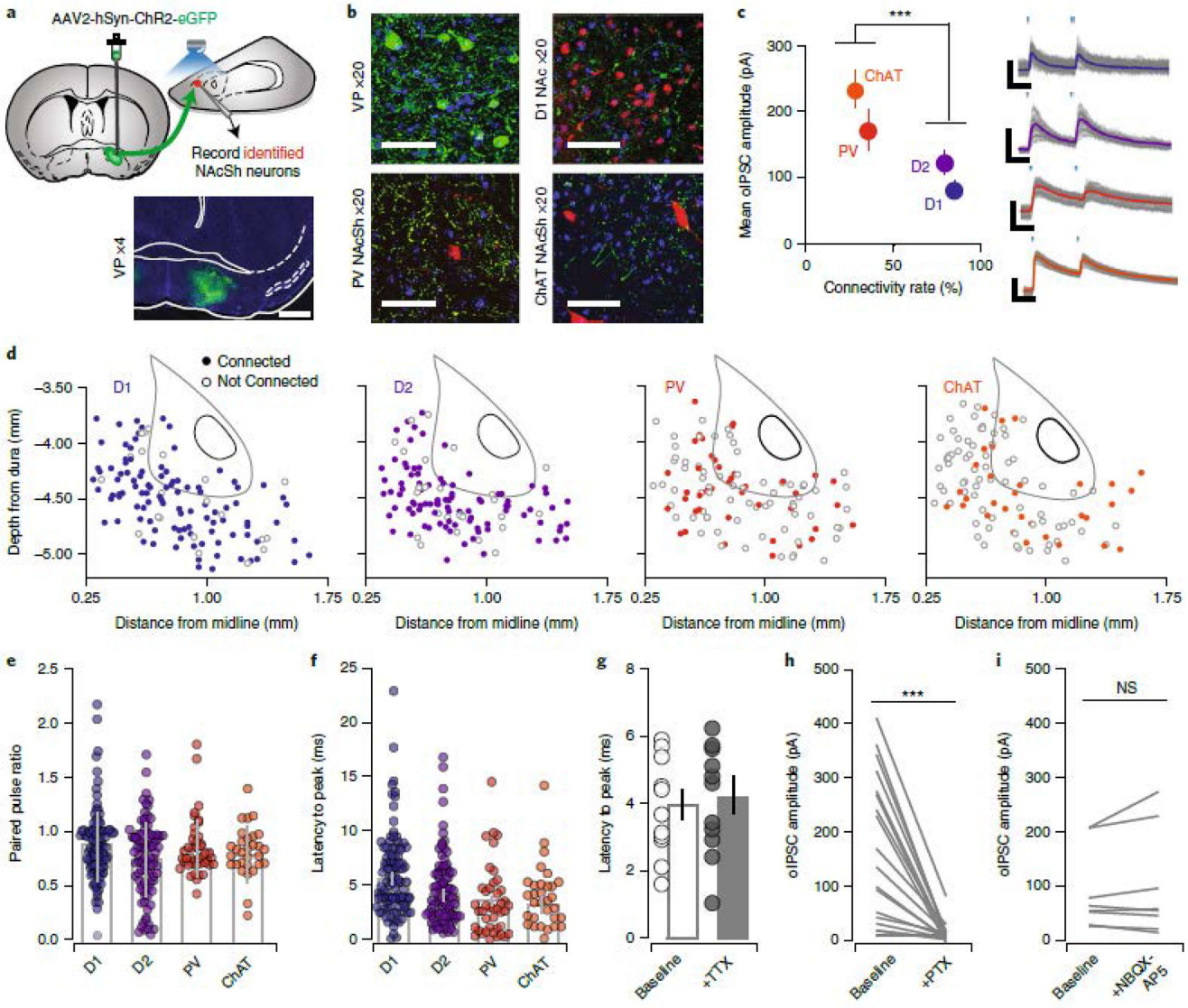

Figure 3. VP neurons make inhibitory, monosynaptic contacts onto NAcSh neurons.

(a) ChR2 was injected into VP in reporter mice (scale bar = 1 mm). **(b)** 20x confocal image of ChR2-infected cells in the VP, ChR2-labelled terminals in the NAcSh in D1-To mice, PV-To mice and ChAT-Cre mice injected with DIO-mCherry in the NAcSh. Scale bar = 50 μM. **(c-d)** Quantification of oIPSCs in D1-MSNs (n=118 cells / 11 mice; 84%, 84.74 ± 8.11 pA), D2-MSNs (n=117 cells / 12 mice; 79%, 114.28 ± 12.23 pA), PVs (n=112 cells / 12 mice; 30%, 163.28 ± 30.70 pA), and CINs (n=104 cells / 10 mice; 28%, 228.65 ± 27.25 pA, Connectivity rate: Pearson x^2 ratio = 106.24, $p<0.001$). Right = representative IPSC traces from each cell type, scale bar = 20 msec, 50 pA. Distribution of recorded neurons throughout the NAcSh for each neural subtype. **(e)** There was no difference in PPR (D1-MSNs = 84.74 ± 8.11, D2-MSNs = 114.28 ± 12.23, PVs = 163.28 ± 30.70, and CINs = 228.65 ± 27.25; $F_3=2.81$, $p = 0.04$, no significant differences by Bonferroni post-hoc test), or **(f)** latency from light onset to oIPSC peak across geneotypes (D1-MSNs: 4.18±0.42, D2-MSNs: 3.77±0.36, PVs: 3.37±0.52, CINs = 3.26±0.34; $F_3=1.81$ $p=0.14$, no significant

differences by Bonferroni post-hoc test). **(g)** Latency to peak was not affected by TTX (Baseline = 16.46 ± 0.69 msec, n=11 cells/5 mice, TTX = 16.15 ± 0.74 msec, t_{11}=0.3113, p = 0.759). **(h)** Currents were abolished by PTX (aCSF = 206.92 ± 37.61 pA, PTX = 24.82 ± 9.88 pA, t_{11}=5.415, p=0.0002, n=12 cells/5 mice) **(i)** but not by co-application of NBQX and APV (aCSF = 324.25 ± 250.89 pA, PTX = 357.86 ± 277.72 pA, t_7=1.215, p=0.264, n=8 cells/5 mice). All bar graphs represent mean ± sem. *p<0.001.

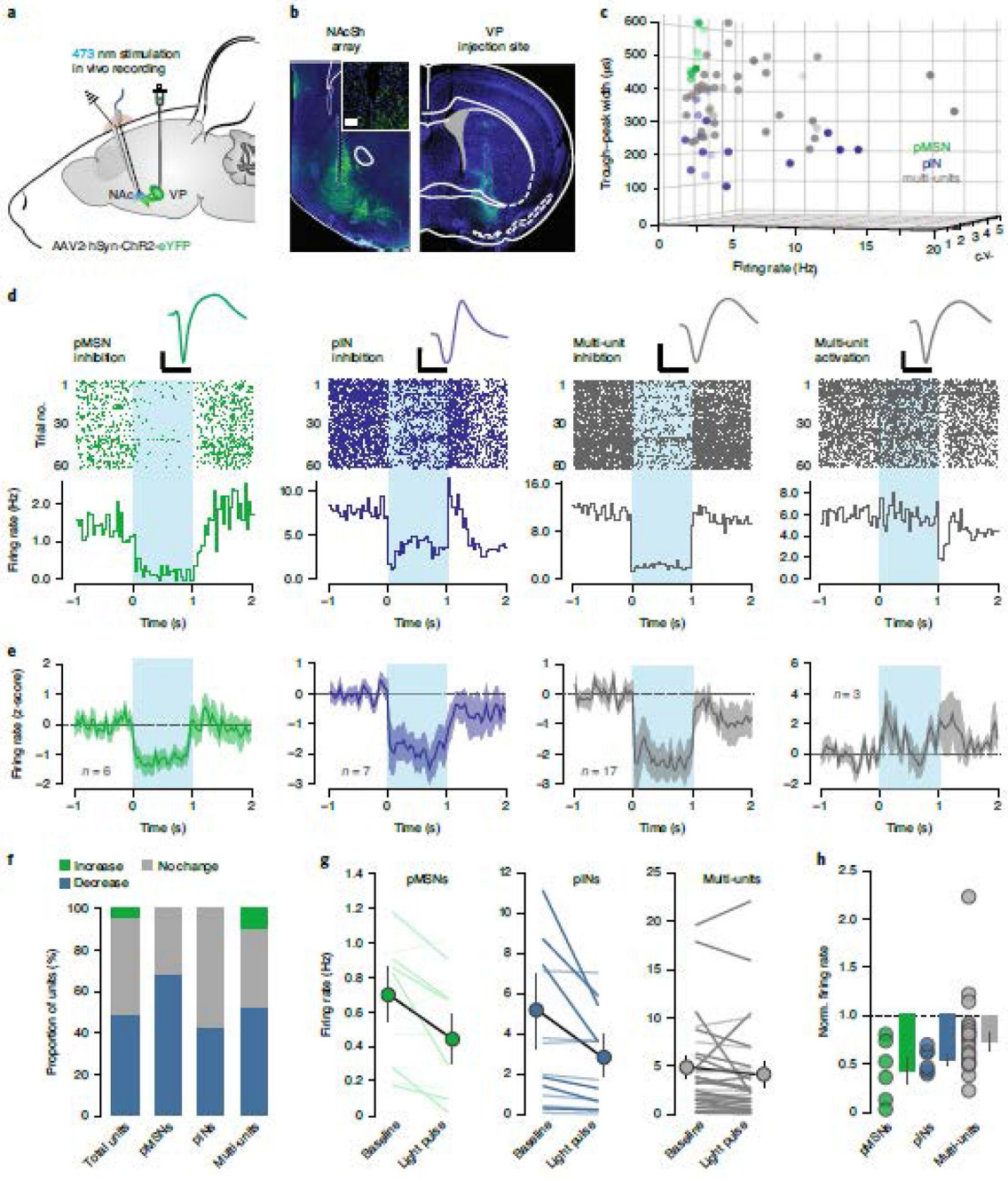

Figure 4. Activation of vArky terminals inhibits NAcSh firing in vivo.

(a) ChR2 was injected in the VP, a recording array with optic fiber was implanted in the NAcSh. **(b)** 4x images of NAc and VP; inset: 20x confocal image of array site. Scale bar = 50 μM. **(c)** Units were classified into clusters by peak-to-valley width, firing rate and CV (n = 9 pMSNs, 14 pINS, 32 multi-units from 6 mice, see Extended data figure 5). **(d-e)** Representative waveform, raster plot and PSTH of single neuron examples (d) and mean ± sem (e) of light-modulated units over 60 trials; 1 sec light pulse is indicated. Scale bar = 500μs, 50μV. **(f)** Proportion of light-modulated units by neural subtype. **(g)** Firing rate

immediately preceding and after light pulse are shown for each cell-type; dark lines: light-modulated units, light lines: non-significantly modulated units (pMSN pre: 0.97 ± 0.11 post: 0.62 ± 0.18, p = 0.015, pINs pre: 4.52 ± 1.68, post: 2.51 ± 0.91, p=0.007, decreased multi-units pre: 4.21 ± 1.12 post: 2.75 ± 0.94, p=0.013, increased multi-units pre: 9.12 ± 5.24 post: 12.13 ± 5.36, p = 0.002). **(h)** Normalized firing rate of all light-modulated units, relative to baseline is shown (pMSNs = 0.46 ± 0.13, multiunits = 0.66 ± 0.05, pINs = 0.59 ± 0.05, F_2 = 1.789, p =0.185).

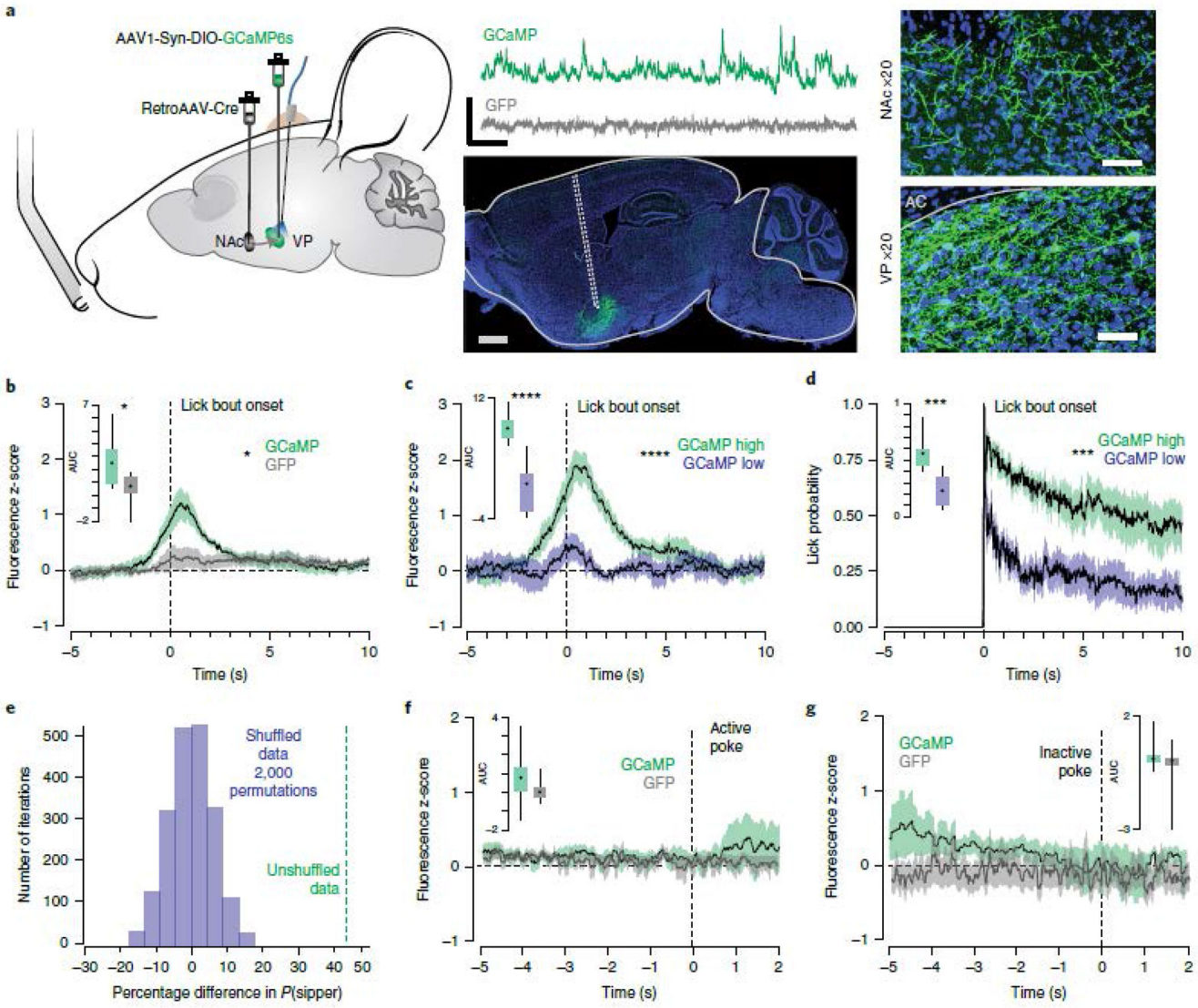

Figure 5. vArky calcium activity is correlated with duration of reward consumption.

(a) retroAAV-Cre was injected into the mNAcSh, AAV-DIO-GCaMP6s was injected in the VP, an optic fiber was implanted in the VP (n=9 GFP / 9 GCaMP, scale bar = 1 mm). Representative traces of Ca^{2+} signal acquired from optic fiber implanted in VP (scale bar=20s, 1 z-score) and 20x confocal images of cell bodies in the VP and terminal fields in the NAc (scale bar=50 μM). **(b)** Combined fluorescence responses from all mice, aligned to onset of lick bout (AUC GCaMP: 2.43±0.75, AUC GFP: 0.52±0.71, F=7.213, p=0.016). **(c)** Fluorescence responses in GCaMP mice, split into upper and lower quartiles based on AUC (44 trials/condition, AUC high trials: 5.76±0.575, AUC low trials: 2.37±0.4911, RM ANOVA, F=13.86, p < 0.0001). **(d)** Licking behavior aligned to bout onset for high- and low-GCaMP signal trials ($AUC_{high\ signal\ trials}$: 5.76±0.57, $AUC_{low\ signal\ trials}$: 2.37±0.49, $F_{High•Low}$=20.08, p<0.001). **(e)** Permutation analysis: distribution of mean difference in lick bout probability between high-and low-VP signal trials with 2000 permutations of shuffled trials ($P_{shuffled}$ (LickBout)VP-Hightrials – $P_{shuffled}$(LickBout)VP-Low trials = 0.6%), mean

difference in real data shown in green (P_{real}(LickBout)VP-High trials – P_{real}(LickBout)VP-Low trials = 42.6%). **(f-g)** GGaMP and GFP signal aligned to active (mean AUC GCaMP: 0.78±0.66, GFP: 0.30±0.46) and inactive nose pokes (mean AUC GCaMP:1.09±0.54, GFP: −0.65±1.56) in an operant task (F_{virus} = 0.58, p=0.46, $F_{active\ v\ inactive}$=1.83, p=0.20). Data represented as mean ± sem. ***p<0.0001.

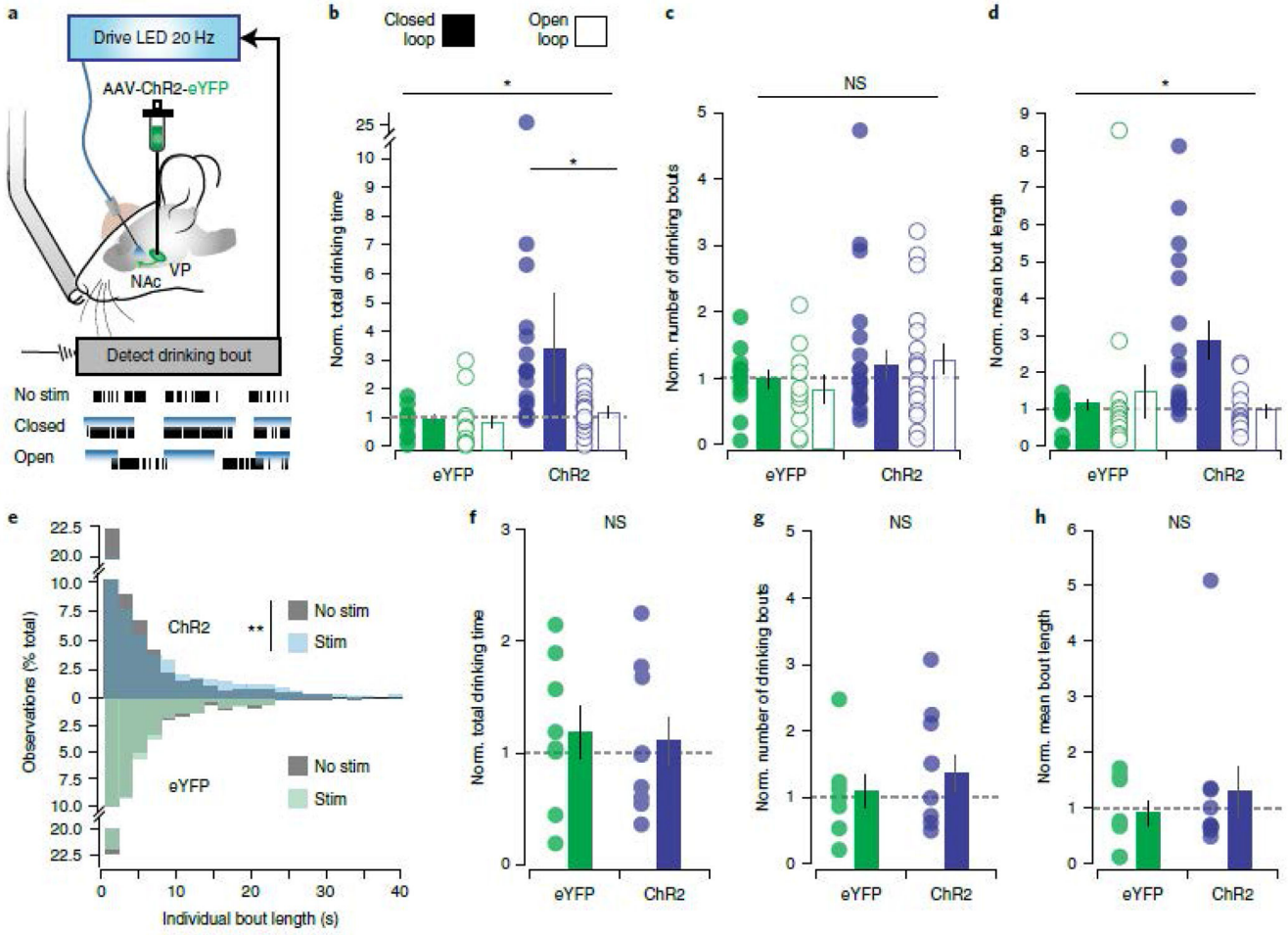

Figure 6. Closed-loop activation of vArky terminals promotes reward consumption.

(a) Optogenetic activation of VP terminals in NAcSh during reward consumption (n=12 eYFP, 18 ChR2) **(b)** Stimulation-induced change from baseline in total drinking time (closed loop: eYFP: 0.95±0.14, ChR2: 3.84±1.32, open loop: eYFP: 0.95±0.14, ChR2: 3.84±1.32, $F_{stim•virus}$ = 4.471, p = 0.016) **(c)** number of drinking bouts (eYFP: 0.98±0.14, ChR2: 1.37±0.25, open loop: eYFP: 0.95±0.14, ChR2: 3.84±1.32, F_{stim} = 0.739, p = 0.482) and **(d)** mean bout length (eYFP: 0.91±0.13, ChR2: 2.83±0.52, open loop: eYFP: 0.95±0.14, ChR2: 3.84±1.32, $F_{virus•stim}$=6.49, p=0.017). **(e)** Histogram distribution of lengths of each individual bout across all subjects ($eYFP_{NoStim/Stim}$ n=564/558, $ChR2_{NoStim/Stim}$ n=1331/1001). **(f-h)** Closed loop optogenetic stimulation did not increase total interaction time (ChR2: 1.14±0.278, eYFP: 1.22±0.239, F1.08834, p=0.312), bout number (ChR2: 1.41±0.278, eYFP: 1.15±0.233, F=2.34582, p=0.145) or mean bout length (ChR2: 1.39±0.432, eYFP: 0.988±0.224, F=1.02321, p=0.327) when a spout without liquid was presented (n = 8 eYFP/8 ChR2). Bars = mean ± sem, *p<0.05.

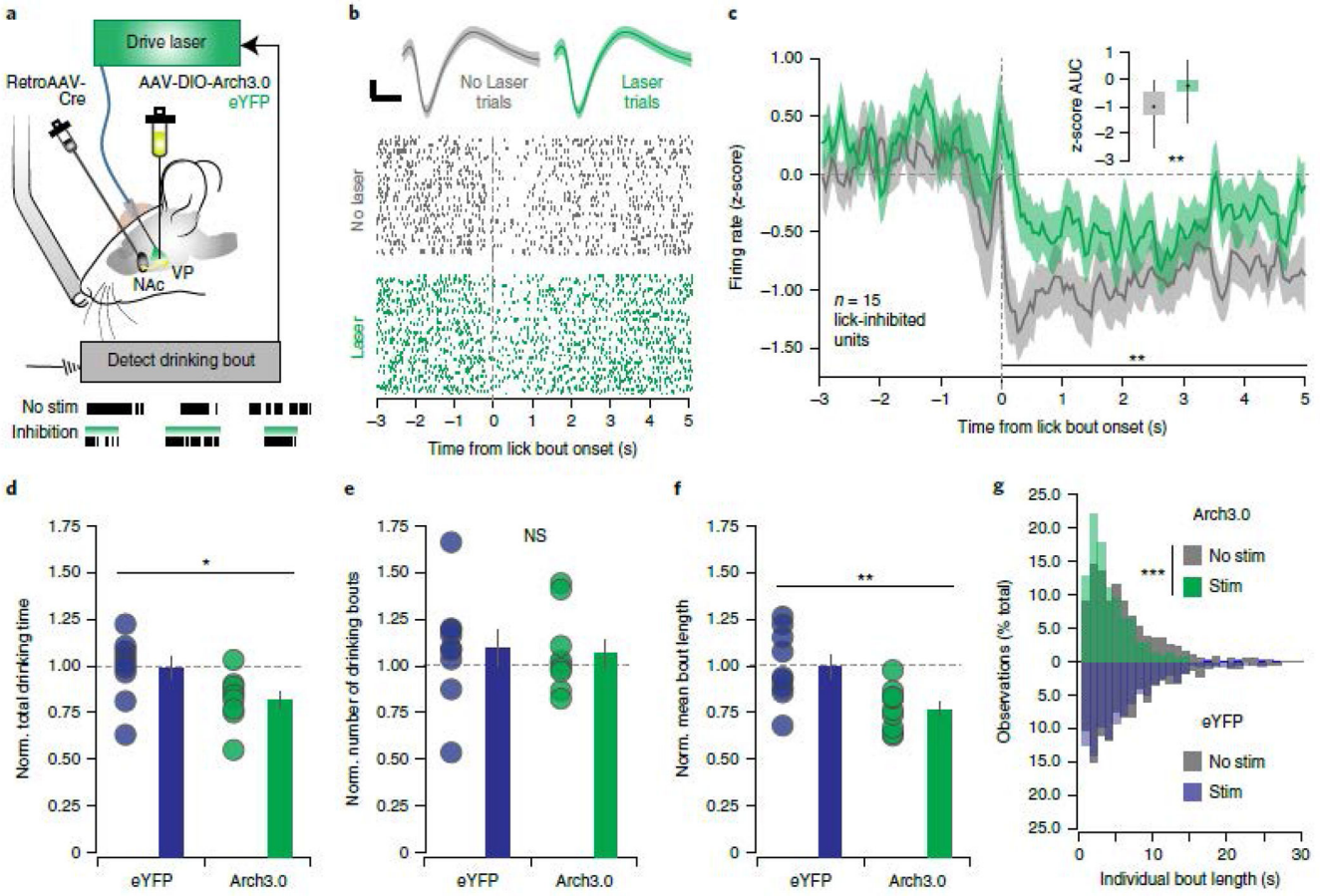

Figure 7. Selective vArky inhibition attenuates consumption-related inhibition of NAcSh firing and reduces length of reward consumption bouts.

(a) Experimental schematic using a retrograde viral strategy to selectively inhibit vArky neurons in a closed-loop manner **(b)** Representative unit waveform and raster plot of firing aligned to drinking bout onset during control trials (NO LASER) and trials where vArky neurons were inhibited (LASER). **(c)** Relative to control trials (−35.5 ± 5.89%), when vArky neurons were inhibited, the consumption-related inhibition of mNAcSh neurons was attenuated (−25.6 ± 4.3%, RMANOVA $F_{Laserxtime}$ = 4.136 p = 0.0018). **(d-f)** Relative to baseline, closed-loop optogenetic inhibition of vArky neurons reduced total drinking time (n=8 eYFP, 12 ARCH, eYFP Pre:158.309 ± 18.1 Post: 156.63 ± 19.17, ARCH Pre: 182.45 ± 13.89 Post:152.58 ± 17.22, $F_{virusxtime}$=6.94 p=0.018), and mean bout length (eYFP Pre: 33.18 ± 3.73 Post: 36.29 ± 5.21 ARCH Pre: 37 ± 4.19, Post: 40.06 ± 5.96, $F_{virusxtime}$=0.01 p=0.981), but not the number of drinking bouts (eYFP Pre: 33.19 ± 3.73 Post: 36.29 ± 5.21 ARCH Pre: 37.00 ± 4.19 Post: 40.06 ± 5.96, $F_{virusxtime}$=0.01 p=0.991). **(g)** Distribution of individual bout lengths with and without laser stimulation (KS eYFP: D=0.098, p=0.201, KS ARCH: D=0.282, p<0.001). Scale bar = 25 μV, 10 msec. Bars = means ± sem. *p<0.01.

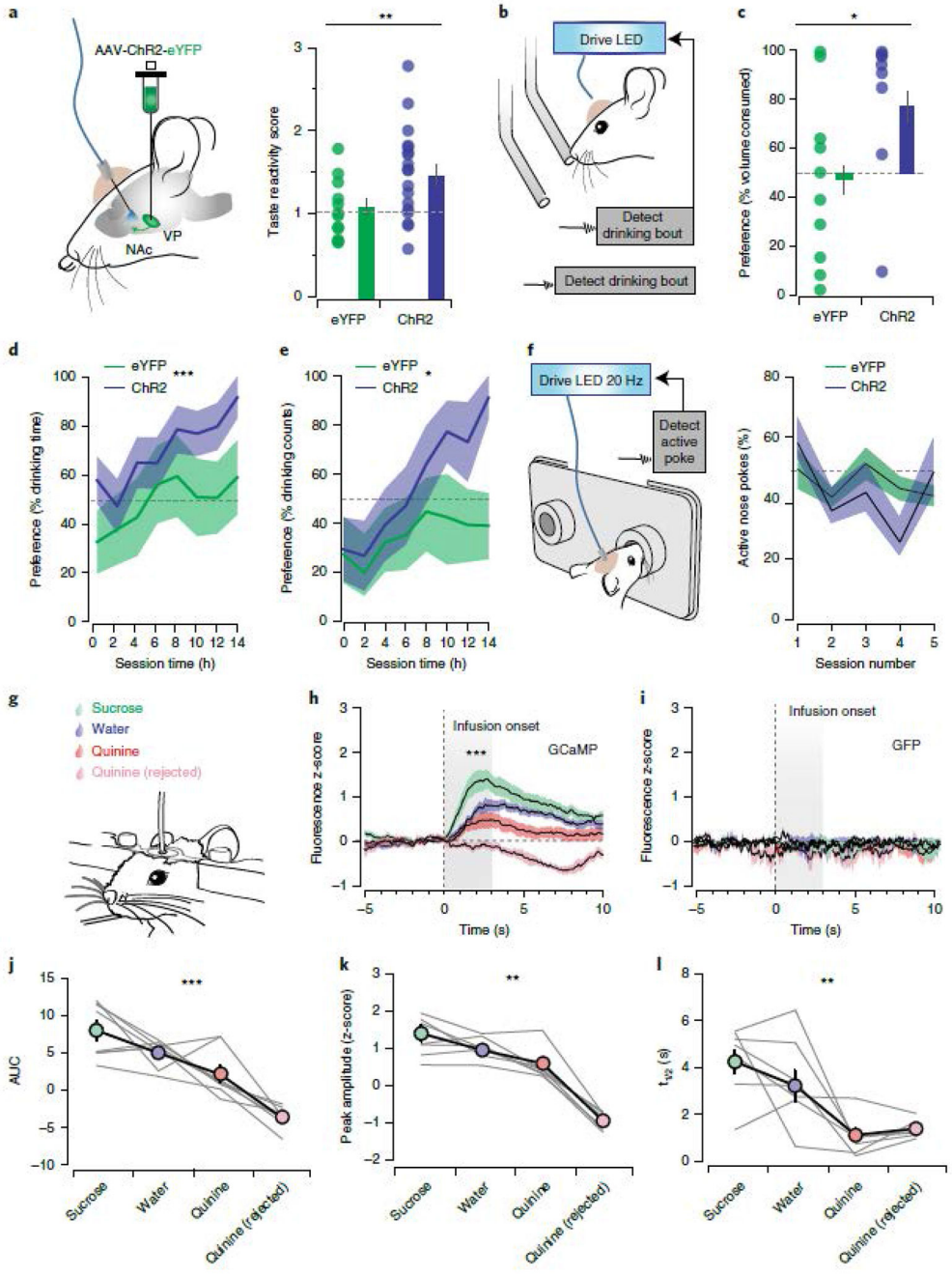

Figure 8. vArky activation enhances reward value and vArky calcium activity scales with reward palatability.

(a) Stimulation-induced change in orofacial taste reactivity ($eYFP_{NoStim}$: 3.88±0.46, $eYFP_{Stim}$: 3.99±0.27, p=0.781, $ChR2_{NoStim}$ = 3.36±0.35, ChR2Stim: 4.77±2.05, $F_{virus•stim}$=7.69, p=0.007). **(b)** Identical rewards were presented in two bottles, one bottle was paired with closed-loop vArky stimulation. **(c)** Preference for stimulated bottle in a two-bottle choice task measured as volume consumed (eYFP: 46±11%, ChR2: 74±12%, x^2=5.05, p=0.025). **(d-e)** Preference for the stimulation-paired bottle in the overnight two-

bottle choice task expressed as proportion of drinking time (F_{virus}=12.5, p=0.0006) and drinking bouts (F_{virus}=6.81, p = 0.010) **(f)** Proportion of active to inactive nose pokes over 5 days of operant training in an ICSS task (eYFP: 44.16±2.08%, ChR2: 41.17±3.47%). **(g)** Head-fixed intraoral infusion of sucrose, water or quinine solutions. **(h-i)** Combined fluorescence responses aligned to onset of solution infusion (GCaMP, AUC Sucrose: 8.03±1.30, AUC Water: 5.03±0.63, AUC Quinine: 2.20±1.13, AUC Quinine rejected: −3.60±0.59; F=42.89, p<0.001). **(j-l)** Transient analysis. AUC of individual mice. Peak Sucrose: 1.39±0.21, Peak Water: 0.95±0.12, Peak Quinine: 0.59±0.15, Peak Quinine Rejected: −0.95±0.9; F=85.04, F=9.43, p=0.0071; $t_{1/2}$ Sucrose: 4.25±0.51, $t_{1/2}$ Water: 3.22±0.65, $t_{1/2}$ Quinine: 1.10±0.28, $t_{1/2}$ Quinine Rejected: 1.38±0.14 F=11.43, p=0.0016. n=8 mice/group, all data presented as mean ± sem.